THERMOELECTRIC COOLING OF A PULSED MODE 1064 nm DIODE
PUMPED Nd:YAG LASER

A THESIS SUBMITTED TO
THE GRADUATE SCHOOL OF NATURAL AND APPLIED SCIENCES
OF
MIDDLE EAST TECHNICAL UNIVERSITY

BY

YÜKSEL YÜKSEL

IN PARTIAL FULLFILLMENT OF THE REQUIREMENTS
FOR
THE DEGREE OF MASTER OF SCIENCE
IN
MECHANICAL ENGINEERING

SEPTEMPER 2010

Approval of the thesis:

THERMOELECTRIC COOLING OF A PULSED MODE 1064 nm DIODE PUMPED Nd: YAG LASER

submitted by **YÜKSEL YÜKSEL** in partial fulfillment of the requirements for the degree of **Master of Science in Mechanical Engineering Department, Middle East Technical University** by,

Prof. Dr. Canan Özgen   _____
Dean, Graduate School of **Natural and Applied Sciences**

Prof. Dr. Suha Oral   _____
Head of Department, **Mechanical Engineering**

Asst. Prof. Dr. Tuba Okutucu Özyurt   _____
Supervisor, **Mechanical Engineering Dept., METU**

Prof. Dr. Rüknettin Oskay   _____
Co-Supervisor, **Mechanical Engineering Dept., METU**

Examining Committee Members:

Asst. Prof. Dr. Cüneyt Sert   _____
Mechanical Engineering Dept., METU

Asst. Prof. Dr. Tuba Okutucu Özyurt   _____
Mechanical Engineering Dept., METU

Prof. Dr. Rüknettin Oskay   _____
Mechanical Engineering Dept., METU

Asst. Prof. Dr. Ahmet Yozgatlıgil   _____
Mechanical Engineering Dept., METU

Murat Şahin, M.S.   _____
Aselsan Inc.

Date: 13.09.2010

I hereby declare that all information in this document has been obtained and presented in accordance with academic rules and ethical conduct. I also declare that, as required by these rules and conduct, I have fully cited and referenced all material and results that are not original to this work.

Name, Last Name   : Yüksel Yüksel

Signature   :

ABSTRACT

THERMOELECTRIC COOLING OF A PULSED MODE 1064 nm DIODE PUMPED Nd:YAG LASER

Yüksel, Yüksel

M.S., Department of Mechanical Engineering

Supervisor: Asst. Prof. Dr. Tuba Okutucu Özyurt

Co-Supervisor: Prof. Dr. Rüknettin Oskay

September 2010, 112 Pages

Since most of the energy input is converted to thermal energy in laser applications, the proper thermal management of laser systems is an important issue. Maintaining the laser diode and crystal temperature distributions in a narrow range during the operation is the most crucial requirement for the cooling of a laser system.

In the present study, thermoelectric cooling (TEC) of a 1064 nm wavelength diode pumped laser source is investigated both experimentally and numerically.

During the heat removal process, the thermal resistance through and between the materials, the proper integration of the TEC assembly, and the heat sink efficiency become important. For the aim of evaluating and further improving the system performance, various assembly configurations, highly conductive components, efficient interface materials and heat sink alternatives are considered.

Several experiments are conducted during the system development stage, and parallel numerical simulations are performed both for comparison and also for providing valuable input for the system design. Results of the experiments and the simulations agree well with each other.

As the laser device works in the transient regime, the experiments and the simulations are also implemented in this regime.

In the final part of the study, the experiments are performed under the actual device working conditions. It is proved that with the designed TEC module and the copper heat sink system, the laser device can operate longer than the required operational time successfully.

Keywords: Diode pumped laser, thermoelectric cooling, TEC integration, heat sink, thermal interface material.

ÖZ

TERMOELEKTRİK SOĞUTUCULARLA DARBELİ, 1064 nm DİYOT POMPALI BİR Nd:YAG LAZERİN SOĞUTULMASI

Yüksel, Yüksel

Yüksek Lisans, Makina Mühendisliği Bölümü

Tez Yöneticisi: Y. Doç. Dr. Tuba Okutucu Özyurt

Ortak Tez Yöneticisi: Prof. Dr. Rüknettin Oskay

Eylül 2010, 112 Sayfa

Lazer uygulamalarında, sisteme sağlanan enerjinin büyük bir kısmı ısıya dönüştüğünden, lazer sistemlerinin ısıl kontrolü önemli bir araştırma konusudur. Diyotların ve kristal parçalarının sıcaklık dağılımlarının dar bir aralıkta tutulması, bir laser sistemin en önemli soğutma gerekliliklerindendir.

Bu çalışmada, 1064 nm dalga boyunda diyot pompalı bir Nd: YAG laserin termoelektrik soğutma (TES) yöntemiyle soğutulması, deneysel ve sayısal olarak incelenmiştir.

Isının sistemden uzaklaştırılması sırasında, malzemelerin kendi içinde ve diğer malzemelerle arasındaki ısıl direnci, termoelektrik soğutucuların düzgün entegrasyonu ve ısı alıcıların verimi önemli hale gelmektedir.

Sistemin performansını incelemek ve daha da geliştirmek adına, olası montaj konfigurasyonları, iletkenliği yüksek malzeme kullanımı, verimli ısıl ara malzemeler, ve ısı alıcı alternatifleri dikkate alınmıştır. Sistemin geliştirilme aşamasında birçok deney yapılmıştır. Bunlara paralel olarak, karşılaştırma ve sistem tasarımına girdi sağlama amacıyla çok sayıda sayısal benzetim çalışması da sürdürülmüştür. Deney ve benzetim çalışmalarının sonuçlarının birbirleri ile uyumlu olduğu görülmüştür.

Lazer cihazı geçici rejimde çalıştığı için deneysel ve sayısal çalışmalar da geçici aralıkta yapılmıştır.

Çalışmanın son aşamasında, deneyler gerçek cihaz çalışma koşullarında gerçekleştirilmiştir. Önerilen TES modulunun ve bakır ısı alıcının kullanımı sayesinde lazer cihazının beklenenden daha uzun sürelerde başarı ile çalışabileceği gösterilmiştir.

Anahtar Kelimeler: Diyot pompalı laser, termoelektrik soğutma, termoelektrik soğutucuların entegrasyonu, ısı alıcı, ısıl arayüz malzemesi.

to my family…

ACKNOWLEDGEMENTS

TABLE OF CONTENTS

LIST OF TABLES

TABLES

LIST OF FIGURES

NOMENCLATURE

c_p	constant pressure specific heat, J/kg K
C.O.P.	coefficient of performance
E	voltage, V
h	convective heat transfer coefficient, W/m^2 K
I	electrical current, A
k	thermal conductivity, W/m K
n	-n type
p	-p type
P	pressure, Pa ; Peltier coefficient , V
Q	heat load, W
R	electrical resistance, Ω
Re	Reynolds number, $Re = \rho\, U\, L\, /\, \mu$
T	temperature, K
v	velocity in longitudinal direction m / s
V	potential difference, V
x	axial coordinate axis
y	vertical coordinate axis
Z	figure of merit, 1/ K

Greek Symbols

α	Seebeck coefficient, V/K
μ	dynamic viscosity, kg/m s
ρ	density, kg/m^3
σ	electrical conductivity, S/m
τ	Thompson coefficient, V/K^2

Subscripts

c	cold side
cond	conductive
conv	convective
f	Fourier heat conduction
h	hot side
H	hot side
in	input
j	Joule heating
L	cold side
leg	thermocouple leg
plate	plate part
xy	x and y material

Superscripts

E	electrical
P	power
R	electrical resistance
T	thermal

CHAPTER 1

INTRODUCTION

1.1 Objectives and Challenges of the Present Study

The primary objective of the present work is to develop a thermoelectric cooling (TEC) system for a diode pumped 1064 nm wavelength infrared laser device. The device is to operate within a targeting pod system. The defined volume and the thermal conditions for the device are to be simulated both experimentally and numerically. Deciding on the laser source components and their configuration, the TEC integration and the heat sink improvement are the main issues in the design. In order to obtain the maximum efficiency out of the laser system, the placement of all the optical, electro optical and mechanical components should be done very carefully. Meeting the system requirements, such as keeping the laser diode and crystal temperatures in a well defined narrow interval, is another important task within the scope of the present study.

Several design alternatives are developed and analyzed to find out the most proper one. The excess heat load on the laser source is removed using thermoelectric coolers in closed control loop. The performance of the TEC modules integrated with the laser source and the heat sink are assessed via experimental and numerical studies.

1.2 Working Principle of Lasers

The word laser is actually the acronym for Light Amplification of Stimulated Emission of Radiation. It is a mechanism that emits visible or invisible light via the

process of stimulated emissions [1]. Light with a specific wavelength passes through the gain medium and is amplified. By the help of oppositely placed mirrors that supply many passes to the light through the gain medium, it is amplified repeatedly. A portion of the light is resonated between the mirrors and escapes as a laser beam from a partially reflective mirror as shown in Figure 1.1.
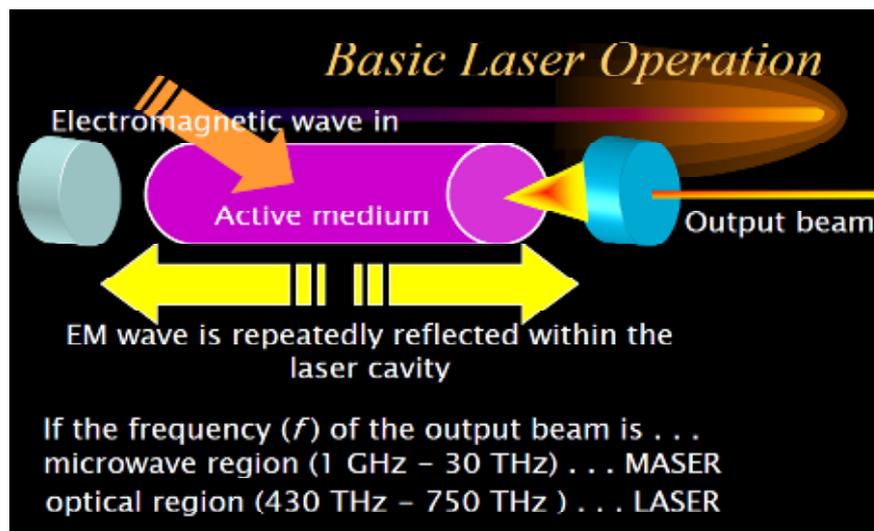
Figure 1.1 Basic Laser Source Unit [2]

The major components of a laser source may be listed as

- the laser medium,
- the stimulating unit,
- the holding and mounting case, the optical elements and mirrors.

In the present work, the laser medium is an Nd: YAG slab in rectangular geometry, and the stimulating unit is a diode pump, a special laser diode which converts electrical energy into light and thermal energy at the same time.

1.3 Cooling Methods for Laser Systems

During their operation, the components of a laser system generate a considerable amount of thermal energy which must be dissipated in order to keep the components within their safe operation temperature limits. The main components which generate heat and cause performance loss and damage are the exciting (stimulating) unit such as a flash lump or diode pumps, and the laser medium which can be a solid state crystal as in the present study, or a liquid or a gaseous medium. Laser cooling techniques can be classified into many different categories but the mostly utilized methods are; the conductive and radiative cooling, passive heat sink cooling, active heat sink cooling, water cooling, phase-change cooling, and heat pipe cooling.

More recently, the Peltier cooling or thermoelectric cooling method is being used beyond the listed conventional methods. Due to its advantages, such as, safety for hazardous electrical environments, precise temperature control, high reliability, small size and volume capacity, low cost, light weight and the solid state construction when compared with conventional cooling techniques, the thermoelectric cooling method is implemented in the present study. Brief information on several cooling methods may be found in the following subsections.

1.3.1 Conductive and Radiative Cooling

Certain laser components, such as the laser cavity body and the optical retainers, are commonly cooled by having them in contact with the holding frame or high volume structure, and/or increasing the surface area which can radiate and exchange heat depending on the radiative characteristic of the components [3]. This type of cooling is commonly used in low power or low frequency pulsed mode laser systems. Since the total heat generation can be compensated by the system volume itself, there is no need for additional cooling out of conduction and radiation [4]. The important point for this type of cooling is that its performance is easily affected by the ambient conditions, the system dimensions and the structure materials.

1.3.2 Passive Heat Sink Cooling

A heat sink is a thermally conductive material which is used for transferring heat from the heat source to the ambient using a relatively large surface area. Passive heat sink cooling is applied by attaching a block of machined or extruded metal to the part that is needed to be cooled. Thermal adhesive materials, such as thermal grease or thermal pad, or a clamping method may be used to place the heat sink under the laser heat source. Certainly, the thermal conductivity of a metal is much higher than that of air, and its ability to radiate heat is better than that of the ambient. This block usually has fins and ridges to increase the heat transfer surface area. Most of the heat sinks used in laser cooling are made of aluminum or copper and attached to the heat sources using a thermal interface material. Passive heat sinks are commonly found in older laser types, in which the parts that do not get very hot and do not require very sensitive temperature distribution for low-power lasers. Passive heat sinks tend to get less effective in time due to the buildup of dust between their metal fins, which reduces the efficiency with which the heat sink transfers heat to the ambient air. The total rate of heat dissipation, the dimensions, the attachment method, type of the convection, and the direction of the airflow are the major factors affecting the selection of the heat sink [5].

1.3.3 Active Heat Sink Cooling

Active heat sinks are the primary cooling equipments in modern laser systems. The method works with the same principle as the passive heat sink cooling, with the addition of a fan which provides air or fluid directed to blow over or through the heat sink. With the forced convection mode of heat transfer enabled by the fans, the thermal management gets easier and the system performance is improved.

Although the active heat sink cooling is more efficient than the passive one, generally the space or power limitations determine the efficiency of the method. The rapid increase in the heat dissipation of high power laser systems makes it inevitable to use fans for thermal solutions. As the laser device volume decreases, the external case surface area decreases and the surface area available for natural convection will

4

not be sufficient for the heat removal. Another common problem in laser applications is the concentration of heat at certain 'hot spots' in the system. These hot spots cause a major challenge while designing the thermal solutions. The use of a fan simplifies the hot spot problems without the need for mechanically redesigning the entire system [6].

1.3.4 Water Cooling

Water cooling is increasing its popularity for the past few years in moderate to high performance laser applications. Water has the ability to dissipate more heat from the cooled parts than various types of metals used as heat sinks. Hence it is suitable for high performance laser applications. One advantage of water cooling is that the cooling system is not limited to a single component but other main heat generating components can also be cooled at the same time [7]. As opposed to air cooling, water cooling is affected less by the ambient temperature. Water cooling has a comparatively low noise-level, hence is favorable for the active cooling of quiet systems. One disadvantage is the potential for a coolant leakage. A leaking coolant can damage electronic components when it comes in contact with them. Another disadvantage is the very high corrosion rate as many metal parts in the system are corrosive [8]. The liquid channels, the expansion chamber and the circulating pumps are some of the additional units for water cooling which increase the volume, the weight, the power requirement and the cost of the entire system. Another drawback of water cooling is its complexity. An active heat sink is much simpler to build, install, and maintain than a water cooling solution [9]. Properly maintained water chemistry in these loops can enhance the reliability and the performance; on the other hand, a poorly designed or maintained water chemistry program may result in a shortened laser life, poor reliability, and interruptions in the operation of the laser.

1.3.5 Phase Change Materials

A phase change material (PCM) is a substance with a high heat of fusion. Hence, while melting and solidifying at certain temperatures, it is capable of storing or releasing high amounts of energy.

Mostly, the solid-liquid phase change is utilized in laser applications. Liquid-gas PCMs are not practical for use in thermal storage due to the large volumes or high pressures required to store the materials when in their gas phase. Liquid-gas PCMs do have a higher heat of transformation than solid-liquid PCMs [10].

Initially, a solid-liquid PCM perform like conventional storage materials; its temperature rises as it absorbs heat. However, unlike the conventional storage materials, when the temperature of a PCM reaches the melting point, it absorbs a high amount of heat without a significant rise in its temperature. When the ambient temperature around the liquid material falls, the PCM solidifies, releasing its stored latent heat [10].

1.3.6 Heat Pipe Cooling

A heat pipe is a hollow tube containing a heat transfer liquid. As the liquid evaporates, it carries heat to the cool end, where it condenses and then returns to the hot end (under capillary action or, in earlier implementations, under gravitation). Heat pipes, thus, have a much higher effective thermal conductivity than solid materials.

All heat pipes have three physical elements in common [11]:
- Container: An evacuated and sealed vessel.
- Working fluid: Differs depending on the operating conditions.
- Wick structure: Provides capillary forces for the liquid to travel in the pipe.

In a heat pipe, the working fluid is vaporized in the evaporator, creating a pressure gradient in the pipe. This pressure gradient forces the vapor to flow through the cooler section where it condenses giving up its latent heat of vaporization. The working fluid is then returned to the evaporator by the capillary forces developed in the wick structure [12].

For use in laser applications, the heat sink on a hot spot region is attached to a larger radiator heat sink. Using heat pipes in addition to an active fan-based cooling keeps the system within its safe operating temperatures.

Heat pipes have no power consumption and light weight which make them favorable in laser cooling. Another important benefit appears when there is not enough space to install a heat sink on the component which dissipates heat. In this situation, a heat pipe can be used to transport heat to a place where it can be dissipated through a heat sink.

1.3.7   Thermoelectric Cooling (Peltier Cooling)

Thermoelectric coolers are essentially solid state heat pumps. They have a similar cooling function as Freon-based refrigerators. Thermal energy is extracted from a region to be cooled, reducing its temperature, and then rejected to a "heat sink" region. The surface of the TEC touching the hot region to be cooled is called the cold junction of the TEC, whereas the surface that is attached to the heat sink is called the hot junction. As opposed to conventional cooling cycles, such as vapor compression refrigeration cycles, thermoelectric coolers have no moving mechanical components or a flowing fluid. Besides that, thermoelectric cooling has analogous parts to the evaporator, compressor and condenser components of a refrigeration system.

The working principle of thermoelectric solid state heat pumps is simply based on the use of thermocouples made of crystalline semiconductor materials [13]. Passing a current through the crystalline semiconductor may generate temperature differential across the thermocouples, as much as up to 70°C.

At the cold junction, the thermal energy is absorbed by electrons as they pass from a low energy level in the p-type semiconductor, to a higher energy level in the n-type semiconductor. The power supply supplies electrical current to move the electrons through the system. At the hot junction, energy is dissipated to a heat sink as electrons move from a high energy level (n-type) to a lower energy level (p-type).

1.4   The Theory of Thermoelectric Cooling
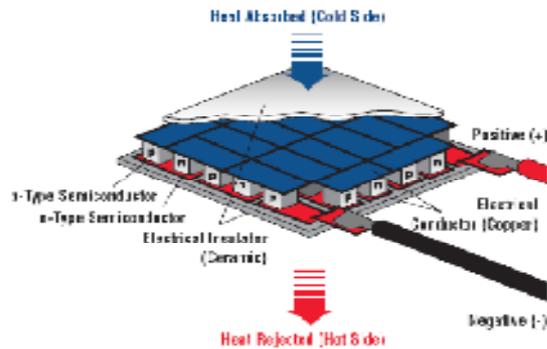
Figure 1.2 Typical Thermoelectric Module Inner Structure

A TEC is a solid-state energy converter. It normally consists of an array of pellets from dissimilar semiconductor material (p and n type), which are thermally joined in parallel and electrically in series as shown in the Figure 1.3. The upper and lower plates are made of ceramic materials which are usually AlO, BeO or AlN alloys [14]. This ceramic structure provides mechanical strength and stiffness besides high thermal conductivity and electrical insulation. The connection between the semiconductor materials and the ceramic portions are done with soldered copper material with high electrical and thermal conductivity. The thermoelectric module (TEM) can be used for cooling, heating, and power generation.

Thermoelectric cooling works with the Peltier effect to creating heat flux between two junctions. Solid state heat pumps have been known since the discovery of the Peltier effect in early 1800s'. The Peltier effect devices became practical only with the development of the semiconductor thermocouple materials in 1900's.

The first important discovery was found in 1821, when a German scientist, Thomas Seebeck, found that an electric current would flow continuously in a closed circuit made up of two dissimilar metals provided that the junctions of the metals were maintained at two different temperatures. Actually Seebeck did not comprehend the

scientific basis of his discovery, however, assumed that flowing heat produced the same effect as flowing electric current. In 1834, a French physicist, Jean Peltier, while investigating the "Seebeck Effect," found that there was an opposite phenomenon where the thermal energy could be absorbed at one dissimilar metal junction and discharged at the other junction when an electric current flowed within the closed circuit. Twenty years later, William Thomson (known as Lord Kelvin) indicated an explanation of the Seebeck and Peltier Effects and described their interrelationship [15]. At that time, however, these phenomena were considered as laboratory applications were not practically applicable.

Today's thermoelectric coolers use modern semiconductor technology where doped semiconductor materials take place of the dissimilar metals which were used in the early thermoelectric experiments.

1.4.1 Seebeck Effect

In order to understand the Seebeck Effect properly, working principle of thermocouples used in measure temperature measurements data may be utilized.
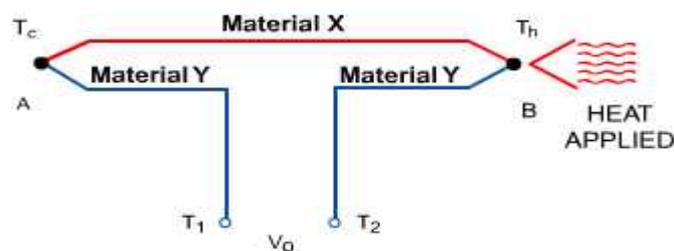
Figure 1.2 Principle of the Seebeck Effect [16]

The idea is that, when two conducting wires of different materials are joined together and heated at one end as shown in Figure 1.4, the temperature gradient results in a potential difference and a continuously flowing current is created which is known as

9

the Seebeck effect. As long as the two ends of the conductor are kept at different temperatures, electron flow inside the conductor will produce an electric field.

The voltage developed between the open ends of the couple is given by $V = \alpha(T_1 - T_2)$ where α is the Seebeck coefficient. For small temperature differences the relationship is linear. The Seebeck effect has two main applications: temperature measurement, and electrical energy generation [17].

1.4.2 Peltier Effect

A thermocouple may also operate in another way when a voltage source is connected across the open ends so that an electric current is driven through the couple. It acts as a heat pump and effectively cools the junction by the Peltier effect.

If the circuit in Figure 1.3 is modified as in Figure 1.4, it is possible to obtain the inverse of the Seebeck effect in the form of the Peltier effect.
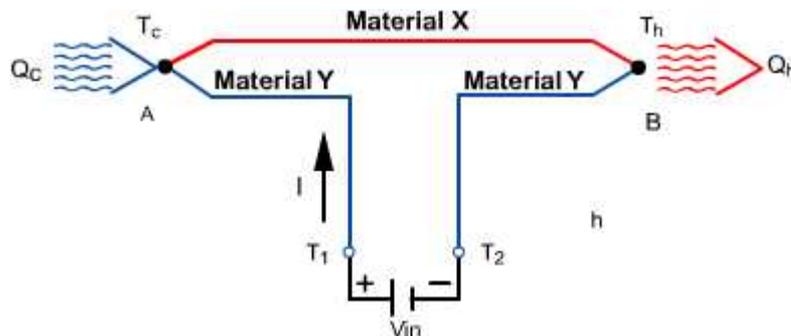
Figure 1.3 Principle of the Peltier Effect [16]

As indicated in Figure 1.4, electric current (I) flows in the circuit, if a voltage (V_{in}) is applied across the end terminals T_1 and T_2. As a result of the current flow, a cooling effect (Q_c) occurs at the thermocouple junction A where the heat is absorbed and a heating effect (Q_h) occurs at junction B where the heat is dissipated. This effect may be reversed with reversing the direction of the electric current in which case the direction of the heat flow will be changed. The Peltier effect can be expressed as:

$$Q_c \left(or\ Q_h \right) = P_{xy} \times I \tag{1.1}$$

where P_{xy} is the differential Peltier coefficient between the two materials, x and y, in volts, I is the electric current flow in Amperes, Q_c and Q_h are the rate of cooling and heating, respectively, in Watts. The Peltier and Seebeck coefficients have a relation given by

$$P_{xy} = T \times \alpha \tag{1.2}$$

In addition joule heating occurs in the conductors as a result of the current flow. It has a magnitude of $I \times R$, R being the electrical resistance, and has an effect opposite to the Peltier effect causing a net reduction in the available cooling.

1.4.3 Thompson Effect

When an electric current is passed through a conductor having a temperature gradient over its length, heat will be either absorbed by or driven from the conductor depending upon the direction of both the electric current and the temperature gradient. The Thompson coefficient is denoted by $\tau = \dfrac{d\alpha}{dT}$ (V/K^2). The Thompson effect plays an unimportant role during the operation of practical thermoelectric modules and is generally ignored.

1.4.4 Performance Measure of a TEC

The coefficient of performance and the thermoelectric efficiency of a thermoelectric device depend on a coefficient called the figure of merit of thermoelectric device. The C.O.P of a TEC can be defined as the ratio of the heat transfer rate absorbed from the cold side to the electrical power input to the TEC. It can be formulated as

$$C.O.P = \frac{Q_c}{V \times I} \tag{1.3}$$

Typical C.O.P values for an efficient TEC vary between 1 and 3. The performance of a thermoelectric material both in cooling (the Peltier effect) and in power generation (the Seebeck effect) is evaluated in terms of the dimensionless figure of merit Z. It is defined as [18]

$$Z = \frac{\alpha^2 \times \sigma}{k} \qquad (1.4)$$

where α is the Seebeck coefficient, σ is the electrical conductivity and k is the thermal conductivity. Often, the dimensionless form ZT, is used where T is the absolute temperature. In order to obtain a highly efficient semiconductor thermoelectric cooler, the figure of merit should be maximized. The studies in the literature are focused on increasing the Seebeck coefficient and reducing the thermal conductivity, especially by manipulating the nanostructure of the materials.

Ideal thermoelectric device is considered to have an infinite electrical conductance and zero thermal conductance. The Joule heating and thermal conductance inside a thermoelectric device cause irreversible energy losses. In order to achieve high efficiency, one should take measures for reducing the temperature differences across the system. In other words, the temperature of the hot side of a thermoelectric device should be as close as possible to that of the heat sink, and the cold side temperature should be as close as possible to the cold sink temperature.

1.4.5 Thermoelectric Materials

The most frequently used semiconductor material in TECs is the bismuth telluride (Bi_2Te_3) alloy which provides individual blocks having distinct "N" and "P" characteristics. Thermoelectric materials are generally fabricated by either directional powder metallurgy or direct crystallization from a molten phase. Each manufacturing method has its own particular advantage, but the directional crystallization of the materials is more common. Some other TEC materials listed as lead telluride (PbTe), silicon bismuth-antimony (Bi-Sb) and silicium-germanium (SiGe) alloys which take different roles in different applications. Thermoelectric modules are designed using

semiconductor materials because of their certain advantages over the bimetallic materials. The lower operating temperature is the only disadvantage of semiconductors. However this can be overcome with the addition of SiC, relatively recent material for high temperature applications [19].

The figure-of-merit of different materials over a range of temperatures can be seen in Figure 1.5. The performance of bismuth telluride peaks within a temperature range that is best suited for most cooling applications.
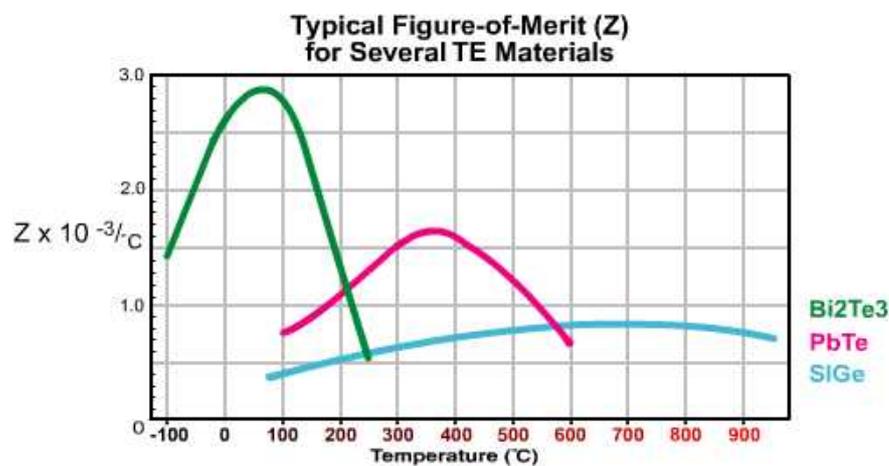
Figure 1.4 Thermoelectric Figure of Merit for Semiconductor Materials [14]

1.5   Advantages of Thermoelectric Cooling

Thermoelectric modules usually provide solutions for low to moderate amount of heat load systems. They provide important advantages over the alternative cooling methods. Significant advantages of TEC modules over the conventional alternatives may be stated as follows:

- **High Reliability and No Moving Parts**: Solid state modules without any moving parts provide maintenance free condition. The operational life is long, typically more than 200,000 hours.

- **Small Volume and Weight**: When compared to the mechanical cooling systems, TEC modules are smaller and lighter. Moreover, special configurations and dimensions are available.

- **Heating and Cooling Ability with the Same Module:** According to the heating or cooling requirements, thermoelectric coolers have the ability to response in both directions simultaneously by tuning the direction of the current using a DC supply.

- **Precise Temperature Control**: TECs can be integrated to open and closed loop control units. This way, it is possible to control and maintain temperatures with accuracy up to +/- 0.1°C.

- **Quiet Operation**: TEC modules generate no electrical noise and can be used with sensitive electronic detectors and sensors. Unlike a mechanical refrigeration system, they are also acoustically silent.

- **Operation in any Orientation:** TECs can be implemented in any orientation and in zero gravity environments. Hence, they are commonly used in many aerospace applications.

- **Target Cooling:** It is possible to control temperature of a single component with TEC modules. A complete packaged assembly can also be cooled via a common base plate.

- **Safety and Environmental Considerations:** Conventional refrigeration systems cannot be fabricated without liquid chemicals that may be harmful to the environment. Thermoelectric devices do not use any kind of hazardous liquids or chemicals as there is no refrigerant involved.

1.6 Disadvantages of Thermoelectric Cooling

TECs have some disadvantages that may be listed as follows:

- **Low to Moderate Heat Removal**: Thermal management of systems with high heat generation is difficult with TEC modules. They are suitable for low to moderate level heat loads.
- **Comparatively Low Efficiency**: C.O.P and efficiency ratios are lower when compared to conventional vapor compression refrigeration cycles.
- **Applicable with DC Current**: Without a DC supply, it is not possible to operate a TEC.

1.7 TEC Application Areas

Since a thermoelectric cooler allows the maintenance the temperature of a structure below the ambient temperature, it can be classified as an active cooler. Also a TEC has the ability to stabilize the temperature of objects that are subjected to varying environment loads and effects. Due to the mentioned advantages over the conventional passive cooling modules such as heat sinks, TECs have a wide spread area of use.

Typical users are military, medical, industrial, consumer, scientific/laboratory, and telecommunications organizations. Usage areas range from beverage and simple food cooling to extremely temperature management systems in missiles and space vehicles. Most single-stage TECs, including high and low current modules, have the ability to remove a maximum of 3 to 6 watts per square centimeter of the module surface area. Multiple modules mounted thermally in parallel may be used to increase the total heat removal performance. In fact, large thermoelectric systems in the kilowatt range have been built for specialized applications such as cooling within submarines and railroad cars [20].

Typical TEC applications may be listed as:

- Aerospace applications (satellites and spacecraft),
- Calorimeters,
- Cold chambers,
- Cold plates,
- Compact heat exchangers,
- Constant temperature baths,
- Dehumidifiers,
- Electronics package pooling,
- Immersion coolers,
- Integrated circuit cooling,
- Infrared detectors,
- Infrared seeking missiles,
- Long lasting cooling devices,
- Low noise amplifiers,
- Microprocessor cooling,
- Night vision devices,
- Thermoelectric generators (recovering waste heat in combustion engines and power plants to produce electric power.),
- Precision device cooling (lasers and microprocessors),
- Refrigerators and on-board refrigeration systems (aircraft, automobile, boat, hotel, portable/picnic, pharmaceutical),
- Thermal viewers and weapons sights,
- Thermal cycling devices (DNA and blood analyzers),
- Water and beverage coolers.

1.8   Literature Survey on Thermoelectric Cooling of Lasers

TEC technique is commonly used in laser systems or subcomponents such as laser collimators which are very sensitive to temperature variations, requiring relatively less cooling capacity but more precise temperature control. For an efficient and high quality laser, it is crucial to maintain the wavelength and the energy output, both strong functions of temperature at desired levels. Open and closed loop temperature optimization may be implemented to laser systems by the TEC usage. Some thermal control compounds such as thermistors, temperature probes and thermocouples can be integrated with the TEC application in laser systems.

Based on the laser system requirements the TEC modules can be constructed in series or parallel configurations. If a high temperature gradient is required, the modules should be applied in series, if a high amount of heat removal rate is required, they should be applied in the parallel configuration.

A microprocessor controlled system is reported in literature for monitoring a thermoelectrically cooled laser diode component with the aid of a temperature sensor. The monitoring provides information on the current temperature and the choice of a proper target temperature to minimize the amount of time to drive the whole system at appropriate temperature levels. The system is very useful for transient systems and has the ability to choose a new target temperature value if the environmental temperature is out of designed level [21].

In another study, a simple TEC element is used in order to maintain the laser diode temperature at a constant value. The main role of the TEC element is preventing laser diode from fluctuating wavelength and output energy when the laser diode heats up. They carried out a safe and reliable optical transmission process with a TEC control circuit composed of a voltage regulator and transceiver units [22].

In another study, the transient working performance of a TEC is increased by tuning the passing current through the TEC [23]. When a higher current density than the optimum SS current is applied to the TEC, it is observed that an instantaneous lower

temperature is reached compared with the SS case. With and without the heat loads the TEC operating conditions are examined by changing the TEC parameters such as the pulse shape, TE element shape, TE element length, minimum achieved temperature, time constant and holding time of min temperatures.
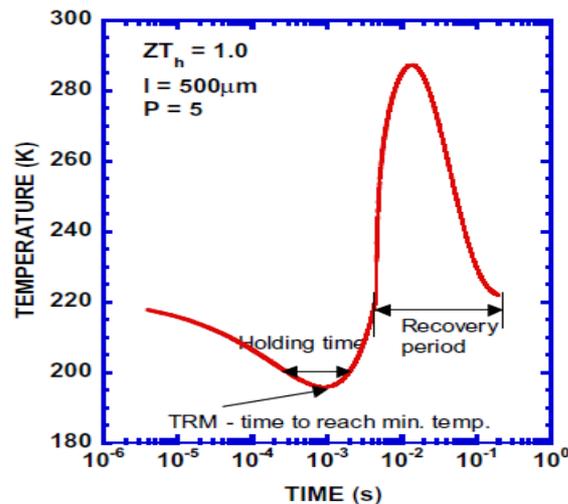
Figure 1.5 Transient Regime Profile with Holding and Recovery Periods

Two cooling regimes uniform cooling and interfacial cooling are identified, and the utilization of the transient cooling effect is established on the time constants for both free standing and passive heat load conditions. Transient temperature and holding time values in Figure 1.6 show that the technique may be applied to microdevices and lower heat loads. However, due to the low holding time, the temperature control of the unit becomes more difficult [23].

In another study, a numerical analysis of the cooling of a laser diode (LD) with a thermoelectric cooler is performed. The thermal characteristics of the laser diode are investigated [24]. Thermal expansion causes changes in the diode shape and position, which also cause serious problems in the light transmission.

18
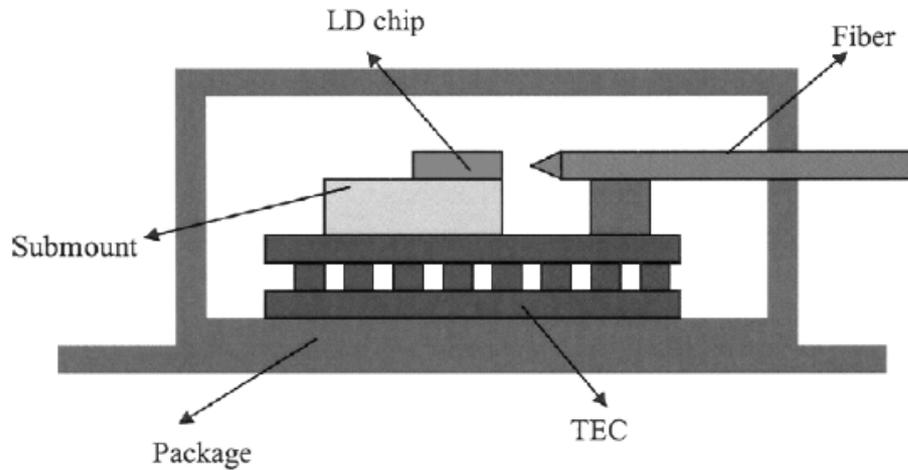
Figure 1.6 Schematic of the Laser Diode Package

An ideal laser diode package is tried to be achieved to maximize the heat transfer from the laser diode. Heat transfer analysis, which includes conduction between the LD assembly and TEC, the natural convection of the filled gas, was performed for a three-dimensional model of the LD and TEC. Radiation heat transfer analysis is not performed in this study [24]. The TECs are modeled by assuming uniform heat load across the bottom and top ceramic plates.

A negative temperature coefficient thermistor (NTC) is mounted near the LD chip. It is used to monitor the internal (submount) temperature. It has been reported that the thermistor resistance decreases with increasing temperature, typically at the rate of 4.4 % per °C. As the temperature inside the laser changes, the thermistor resistance change is translated into the current supply to the TEC [22].

They observed that;

- The temperature difference between the LD and the LD submount and the TEC is several Kelvins in spite of the short distance. Therefore, the contact should be designed carefully.

19

- The temperature of the LD and thermistor changes linearly hence reading the LD temperature from the thermistor is reasonable.

- The ascending heat rate of the LD causes TEC to descend the cooling capacity.

- The ascending TEC current flow provides higher cooling capacity in total.

- The effect of natural convection by the filled gas is negligible under the operational conditions.

In another work, some spreading materials are applied in order to decrease the thermal resistance between the TEC module and the ambient. Spreading materials also increase the C.O.P of the TEC modules. The proposed cooling system includes a spreading device (copper block, vapor chamber, heat pipe, thermosiphon, or cold plate) used for uniform heat spreading on the cold side of the TEC. A heat sink/remote heat exchanger/cold plate is attached to the hot side of the TEC to dissipate the CPU heat load.

It is observed that using different spreading devices, substantial performance improvement can be achieved. The heat sink to ambient thermal resistance can be improved by more than 40-60% if the TECs are optimized over a range of reasonable boundary conditions and applying suitable phase change spreading devices [25].

1.9 TEC Device Selection Method

The selection of a proper thermoelectric cooler needs an overall evaluation of the system in which it will be used. Mostly, it is possible to use one of the standard modules however in some cases a special design may be needed to meet the mechanical, electrical and other requirements. Usually, the design and selection of a TEC module is performed according to the supplier's product performance curves. The design starts with determining the cold and hot side temperatures of the TEC, especially in order to find the temperature gradient between these surfaces. After that the amount of heat released from the cold side is calculated.

The main three parameters for the TEC selection are [26]

- T_c (TEC's cold side temperature)
- T_h (TEC's hot side temperature)
- Q_c (The amount of heat released from cold side)

While determining the T_c parameter, if the cooled object is in direct contact with the cold surface of TEC, the required temperature of the cold surface of the TEC, T_c can be taken as desired temperature of the cooled object. If an ambient volume or far object to the cold surface is cooled, the total thermal resistance between object and TEC should be considered when deciding on the T_c.

When determining the hot surface temperature T_h, two major parameters must be taken into account:

1) The ambient environment temperature that the heat load is being rejected.
2) The efficiency of the heat exchanger used between hot surface of the TEC and the ambient temperature.

The two parameters directly affect the thermal resistance between the hot surface and the ambient. As long as the thermal resistance is kept low, the hot side temperature should not be very high value. During this stage of the design, T_h parameter should be selected based on the total heat load that should be removed through the heat sink to the ambient is equal to $Q_h = Q_c + VI_c$. It means that total the heat load also includes the electrical power input.

In TEC modules, the heat sink or cold plate components rejecting heat to the ambient are very important. Air to air, air to water, water to air, water to water and cold plate cooling units are available. The most suitable heat sink should be selected so that the total thermal resistance is maintained in the operational region.

21

The amount of heat to be removed by the cold surface of the TEC is the most difficult parameter to determine. All the thermal loads on the TEC should be considered. These loads can be of any type from electronic devices and conduction through any warmer object in contact with the cold surface. (i.e. electrical loads, insulation, air surrounding objects, mechanical fasteners, etc). In some cases radiative heat transfer effects must also be considered.

Once the main three parameters are determined, the proper TEC is selected using the performance curves. One can find the intersecting current line with the already calculated ΔT and Q_c values in Figure 1.8. After finding the current value, Figure 1.9 is used to find the required system voltage.

From the Figure 1.8 it can be observed that for every current line, the maximum temperature gradient (ΔT) is obtained when $Q_c = 0$ W. Likewise, for every current line, the maximum heat removed from the cold side (Q_c) is obtained when $\Delta T = 0°C$.
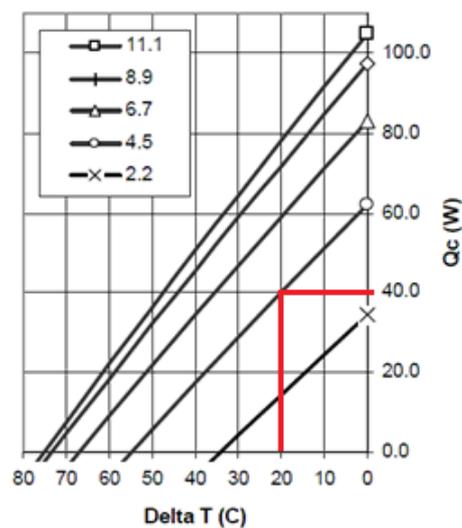
Figure 1.7 ΔT versus Q_c at varying I_c values
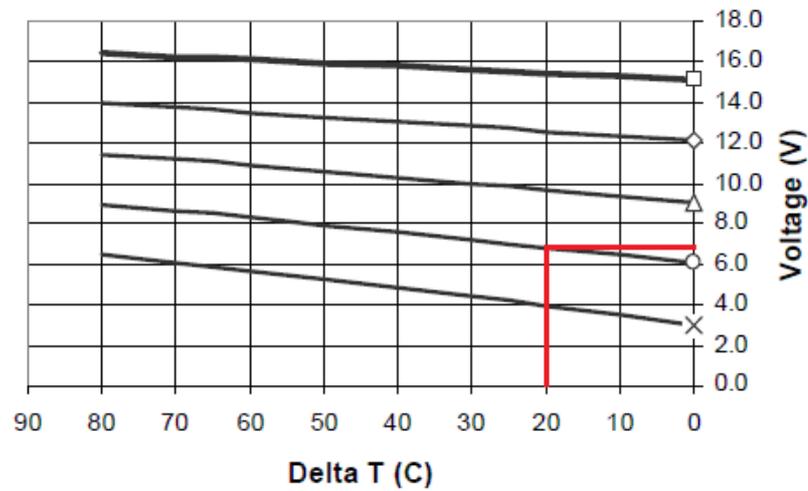
Figure 1.8 ΔT versus Voltage at Varying I_c Values

1.10 The Outline of the Thesis

In this thesis, an experimental investigation of a thermoelectrically cooled diode pumped laser device is performed. In order to help the design of the laser source, the TEC assembly and the heat sink components, the experimental studies are supported with numerical simulations. The outline of the thesis in this respect is as follows.

Firstly, the generated heat load in the laser source is calculated analytically. Depending on the distribution of the heat load, the most suitable laser source configuration is tried to be determined in Chapter 2. Moreover, the TEC module with the heat sink system is formed by applying the TEC assembly rules.

In Chapter 3, the construction of the laser pumping chamber on the TEC - heat sink assembly is presented. Electrical resistances are used to simulate the heat generating components. The effects of the ambient air, the air flow rate and the heat load on the TEC cooling system are observed. A parallel TEC module embedded numerical simulation is also driven to compare the results and to assess the surface contact resistance between the components.

After obtaining important feedbacks on the TEC performance, TEC integration method and the designed laser components are presented in Chapter 4. Moreover, the final numerical heat sink model is created implementing the material and the fin geometry.

In Chapter 5, the construction of the complete device experimental set up with the newly manufactured laser source components and the heat sink is explained. All the devices used in the POD system are manufactured using rapid prototyping techniques in order to increase the reliability of the experiments. The environmental cooling unit which supplies conditioned air to the POD is represented by resistance heaters, fan and other necessary duct components.

Finally, the discussion of the results and conclusions are given in Chapter 6. In addition, the laser device operational conditions are discussed, and suggestions for a future work are stated in this chapter.

CHAPTER 2

HEAT LOAD CALCULATION AND CONSTRUCTION OF THE LASER PUMPING CHAMBER

As it is mentioned previously, the laser pumping chamber has main mechanical components which act as heat generators, absorbers and carriers during the operation. Before the numerical or experimental studies, the system heat load and operating temperatures should be known for defining the correct boundary conditions.

In diode pumped laser systems the main heat sources are the pumping diodes which convert electrical energy into optical energy. Some of the optical energy out of totally 10 diodes is absorbed by the Nd: YAG laser crystal and again some of them will be given out as a final laser beam from crystal. The rest of the optical energy coming from diodes is also absorbed by optical holders and components surrounding the laser source.

All the heat load calculations are performed by analytically using the working specifications of the laser diodes based on a similar diode pumped laser study [27]. The heat load calculations are done according to the construction of laser pumping chamber.

Laser crystal is mounted on a flat surface and is excited by 10 laser diodes (5 on each side). All the diodes are mounted equally in both sides on same type of diode holders which are also integrated on the single base plate. As it can be seen in the Figure 2.1, active cooling is performed by integrating the cold sides of TEC modules with the common base plate. This way a number of critical components may be cooled at the

same time. The critical components are the laser diodes and mounting parts of the laser crystal in order to maintain a stable temperature distribution.
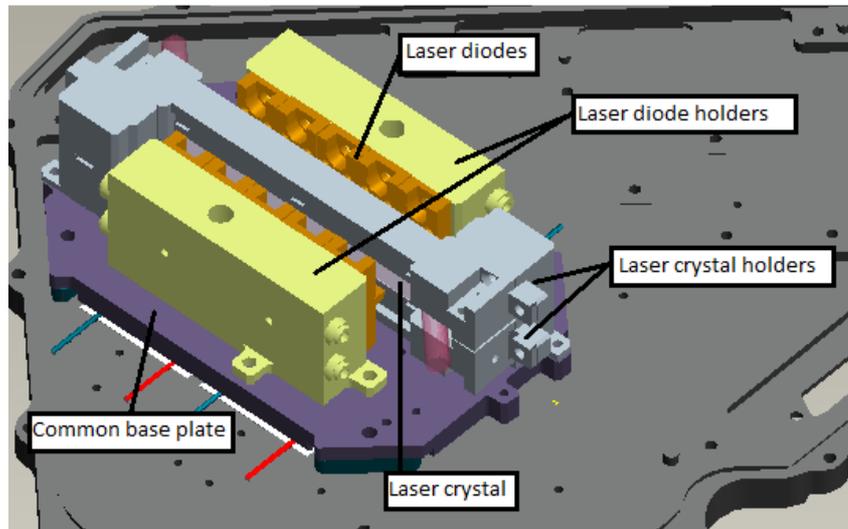
Figure 2.1 The Construction of Laser Pumping Chamber

2.1 Calculation of the Heat Load in the Laser Source

The working specifications of the laser system may be summarized as follows:

- 200 µs pulse width operating mode at 1, 10 and 20 Hz repetition rates.
- 808 nm wavelength stimulating diode laser beam out of total 10 diode pumps.
- 1064 nm wavelength infrared laser, as the final laser beam shall be obtained.

For the heat load calculations, firstly the electrical energy provided to the diodes is calculated and this value is considered as the total energy /supplied to the system. The entire energy is divided mainly into three portions. The energy accumulated in the diode mounting parts, in the laser crystal and in the surrounding components.

To be on the safe side, calculations are performed based on the maximum heat generation mode which corresponds to 20 Hz repetition rate operational condition. If

the cooling system is designed according to this 20 Hz case, the other 10 Hz and 1 Hz modes are automatically satisfied.

The electrical energy is converted into heat and optical energy. Some of the optical energy is absorbed by laser crystal and the rest remains on the diode holders. This remaining heat load is determined from the supplied information by the manufacturer of the diodes. In laboratory conditions and in the operating temperature ranges, laser diodes are reported to work with %45 efficiency [28].

- The electrical power supplied to the laser diodes may be calculated for continuous operation as

$$100\text{A} \times 14\text{V} \times 10\text{pieces} = 14000\text{W} \qquad (2.1)$$

For the pulsed mode operation the average power is

$$14000\text{W} \times 200 \times 10^{-6}\,\mu\text{s} \times 20\text{Hz} = 56\text{W} \qquad (2.2)$$

- The remaining heat load on the diode mounting components is

$$14000\text{W} \times (1 - 0.45) = 7700\text{W} \quad \text{for continuous operation,} \qquad (2.3)$$

$$7700\text{W} \times 200 \times 10^{-6}\,\mu\text{s} \times 20\text{Hz} = 30.8\text{W for pulsed mode (average power)} \qquad (2.4)$$

The heat accumulated in the laser crystal is also used as an input parameter for numerical analysis. By considering the absorptivity, transmissivity and reflectivity coefficient of laser crystal, %30 percent of the total excitation energy is assumed to be accumulated in the crystal based on a similar study [29]. It can be calculated as

$$14000\text{W} \times 0.45 \times 0.30 = 1890\text{W} \quad \text{for continuous operation,} \qquad (2.5)$$

$$1890\text{W} \times 200 \times 10^{-6} \, \mu\text{s} \times 20\text{Hz} = 7.6\text{W} \quad \text{for pulsed mode (average power)} \quad (2.6)$$

At this point the final laser output should also be calculated.

For every pulse 120 mJ laser energy is given out as laser pulses and the average laser power is calculated as

$$120\text{mJ} \times 10^{-3} \times 20\text{Hz} = 2.4\text{W} \qquad (2.7)$$

During the operation the net average heat load on the laser crystal is

$$7.6\text{W} - 2.4\text{W} = 5.2\text{W} \qquad (2.8)$$

- The optical energy absorbed by the system components is;

$$14000\text{W} - 7700\text{W} - 1890\text{W} = 4410\text{W} \quad \text{for continuous operation,} \qquad (2.9)$$

$$4410\text{W} \times 200 \times 10^{-6} \, \mu\text{s} \times 20\text{Hz} = 17.6\text{W} \quad \text{for pulsed mode (average power)} \qquad (2.10)$$

- The total heat accumulated in the system is

$$30.8\text{W} + 5.2\text{W} + 17.6\text{W} = 53.6\text{W} \qquad (2.11)$$

This is nearly the same with previously calculated total electrical power coming from the diodes by adding the outgoing laser power.

2.2   CFD Analysis during the Design Stages

In order to decide on the most reasonable cooling system configuration, the temperature stabilities of the diodes and the laser crystal have been investigated. Predetermined heat loads and thermal boundary conditions are used in this analysis.

28

Mechanical components and assemblies were not constructed until the most logical configuration is achieved based on the CFD analysis.

Numerical simulations are performed with the IcePak software which is one of the useful ANSYS software used especially in electronic cooling problems. Since there is a macro written for TEC modules, running TEC embedded analysis with Melcor TEC library is possible [30]. IcePak is used while creating the model of the laser pumping chamber; however, Fluent is preferred to observe the temperature distribution on the heat sink plate.

Since the project needs multidisciplinary studies, design, manufacturing and CFD analyses have been performed by different teams in MGEO Division at ASELSAN INC.

Thermal management of these components has a big importance to achieve satisfactory performance and reliability of the laser module. Laser wavelength, quality and output power is directly affected with thermal management.

The laser crystal is represented in Figure 2.2. Some conditions on the laser crystal may be stated as follows.

- The laser crystal should have a temperature distribution in z-direction as uniform as possible. Since the generated laser is propagating in the x-direction, a nonuniform temperature distribution in that direction is compensated by the zigzag form of the laser profile [27]. The optical behavior of the laser crystal is affected dominantly by different thermal conditions in the z-direction. Laser crystal should be excited by the diodes from lateral directions as symmetrically as possible.

- Its temperature should not exceed 120°C which is assumed to be a safe temperature value in this study [31].

- It should have a fixed placement during operation and while being exposed to high mechanical and thermal loads. Some mechanical fasteners can be used for fixing, in addition to chemical adhesives, pads or tapes.
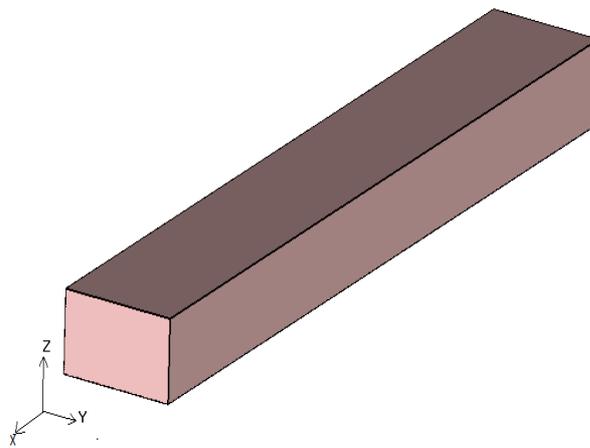
Figure 2.2 Laser Crystal with its Coordinates

In addition, the diodes

- should be maintained at 50 ±3°C in order to get the 808 ±5 nm exciting laser beam [32];

- should be placed symmetrically on the carrier parts with small position tolerance deviations;

- should have a fixed placement during the operation and while being exposed to high mechanical and thermal loads.

2.3   Applications of the Laser Source Configuration

After selecting a reasonable configuration, a number of numerical and experimental analyses have been performed. Due to the short operating time, transient regime is considered.

The cooling principle of a TEC is based on removing heat from a cold plate to a heat sink. TEC has two different temperature surfaces with temperatures T_c and T_h. The heated part is connected to the T_c side and the T_h side is joined with a heat sink or a cold plate.

Before deciding on the final geometry of the mounting base plate and the heat sink, a series of experiments have been conducted with the firstly manufactured copper mounting hot plate as shown in Figure 2.3.
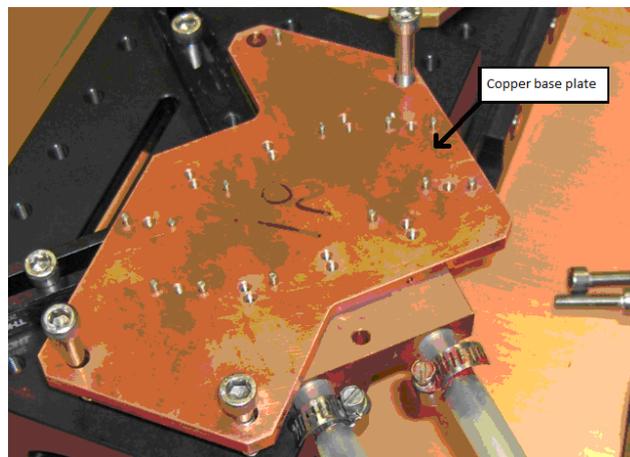
Figure 2.3 Mounting Base Plate

The first tests have been carried out using available materials in clean laboratory condition. The interface material is a product of Laird Technology T-grease 2500. TEC devices are integrated one by one in order to maintain the system tolerance at good levels.

The low temperature of the cold plate compensates the high thermal resistance between the hot and the cold plate. At this stage, four TEC modules have been

sandwiched between the hot and the cold plate. The necessary contact pressure, rigidity and the stiffness has been maintained with four clamping M5 screws as in Figure 2.4.
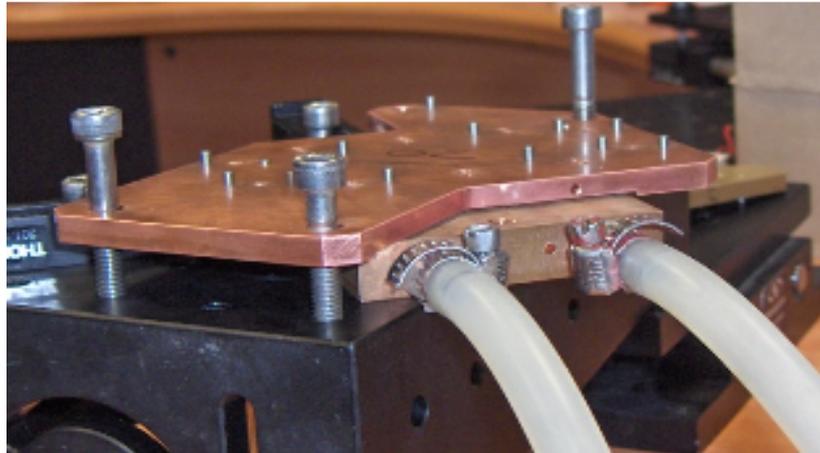
Figure 2.4 Base Plate, TEC Module and Liquid Cooled Cold Plate Assembly

For mounting the necessary laser source components at first, the diode holders which are already assembled with 10 diodes have been integrated with system shown in Figure 2.5.
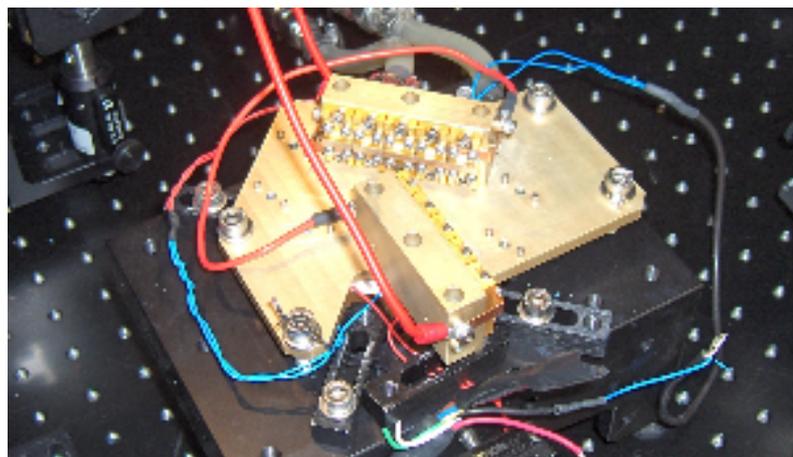
Figure 2.5 Diode Holders and Base Plate Assembly

In Figure 2.6 one can see the laser crystal mounting components. The laser crystal has been placed on mechanical component with a thermal pad in order to provide

high heat transfer rate from crystal. In addition, the thermal pads prevent crystal from probable cracks and breaks because of the thermal expansion difference between the metal and crystal at high temperatures.

Figure 2.6 Laser Crystal Mounting Components

Once the completed laser crystal system became ready to be mounted on the base plate the required laser source geometry has been formed as shown in Figure 2.7.
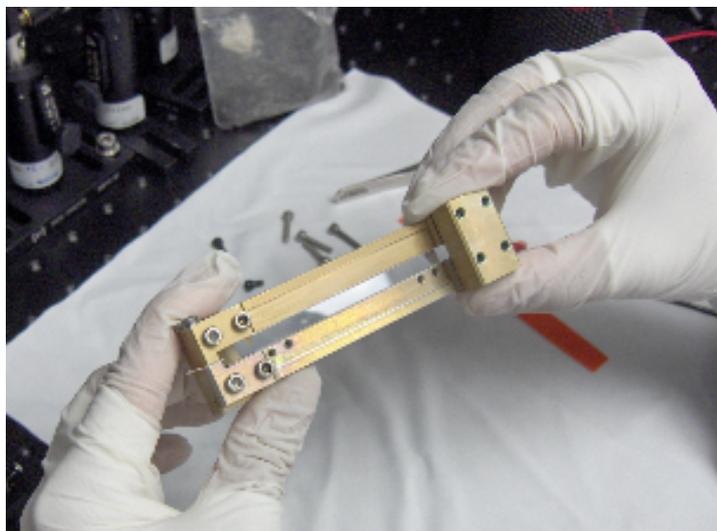
Figure 2.7 Completed Laser Crystal Holder System

In Figure 2.8, the completed laser pumping chamber unit is presented.
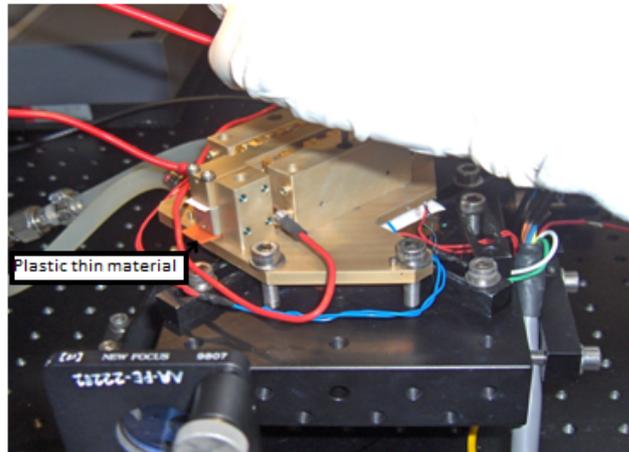
Figure 2.8 Completed Laser Pumping Chamber

2.4   Assembly Procedure of TEC Module

The integration of the TEC into system is very critical. It is required to select the correct type and configuration of the TEC. They are very sensitive to the environmental conditions, therefore every affecting parameters should be considered carefully in every stage. The techniques used in the assembly of a thermoelectric system can be as important as the selection of the proper TEC device. The purpose of the TEC assembly is namely to remove heat. Generally a TEC device, in the cooling mode, transfers heat from heat source to the ambient. All of the mechanical interfaces between the objects to be cooled and the ambient are also thermal interfaces. Similarly all thermal interfaces tend to inhibit the heat flow or add thermal resistance. When considering assembly techniques, every reasonable effort should be made to minimize the thermal resistance.

Since the cooling capacity of the cold plate is higher than that of the forced air cooled heat sink, the system set up should be constructed with active cooled heat sink and fan parts.

In order to increase efficiency, the following assembling steps have to be followed;

Firstly, thermoelectric module, heat exchanger and cold surface should be cleaned and degreased with methanol or other chemicals. The mechanical profile and flatness tolerances for the hot plate and the TEC contacting surfaces should not exceed 0.075 mm.

As it can be seen from Figure 2.9, the hot spots of the base plate are already machined. This way, the TECs can be integrated with the ease of taking reference from the machined features.

Figure 2.9 Cleaned and Degreased Base Plate

The interface material between the ambient and the heat source is very important. The air gaps between the contacts and the surface irregularities cause an increase in the thermal resistance. For this assembly two types of interface materials are used. One is thermal grease and the other is a thermal pad. Moreover, thermal pad is simple to use and not very dirty.

Table 2.1 Thermal Properties of the Interface Materials

Material	Thickness (mm)	Thermal Conductivity (W/m K)	Thermal Impedance ($°C\,m^2\,/\,W$)
Laird T2500 T-grease	0.025	3.8	1.0 e-4
Alfatec Thermal Pad	0.225	2.7	9 e-5

Some other interface materials according different use of areas and suitable for this application are;

- eGraf 1205 (Highly conductive, low thermal impedance, flexible),
- Choterm T500 (Moderate thermal conductivity, flexible),
- Thermattach tapes (Low thermal conductivity compared to other but two stick sides available for stiffer integration),
- Wakefield type 120 and Dow type 340 thermal greases.

Both interface materials and thermal greases should be used with clamping elements. Another way is to directly apply the adhesive without any fastener but it is more challenging and in the case of wrong placement it is hard to fix back.

The thermal grease is applied gradually and its thickness is measured until the necessary value is obtained. The maximum thickness should be limited to 0.025 mm. At the end, a thin continuous film of thermal grease should be obtained as in Figure 2.10.
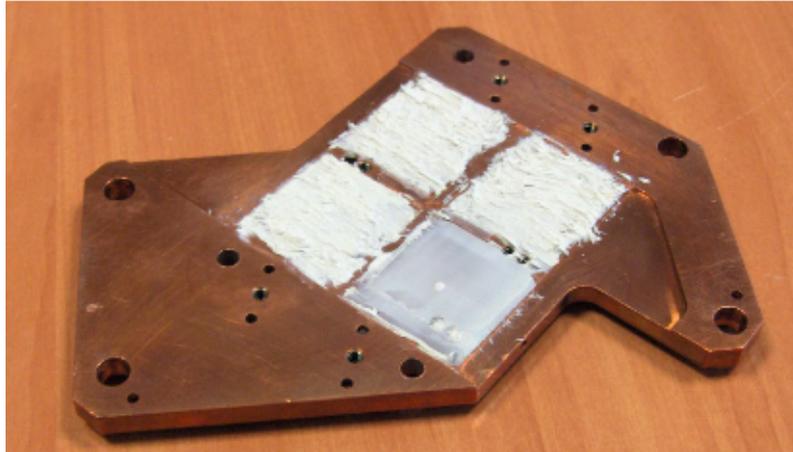
Figure 2.10 Application of the Thermal Grease on the Base Plate

The thermal grease is also applied on the T_c side of the TEC. This provides more uniform contact for two surfaces and yields more homogeneous interface structure as shown in Figure 2.11.

Figure 2.11 Application of the Thermal Grease on the TEC Surface

The thermal grease should only be applied to the necessary outer surface. The inner semiconductor structure should not get in contact with thermal grease. If this contact happens there can be electrical and thermal short circuits between the n- and p- type

semiconductors (between the hot and cold surfaces) which can change the TEC efficiency.

As illustrated in Figure 2.12, a one side pressure sensitive thermal pad is used to make contact between the TEC and the heat sink. Once the thermal grease is applied to the T_c surface, pressure adhesive bonding side of thermal pad is applied to the T_h surface. Then, the TEC module is integrated to the base plate from its cold side by gently oscillating the module back and forth, exerting uniform downward pressure.
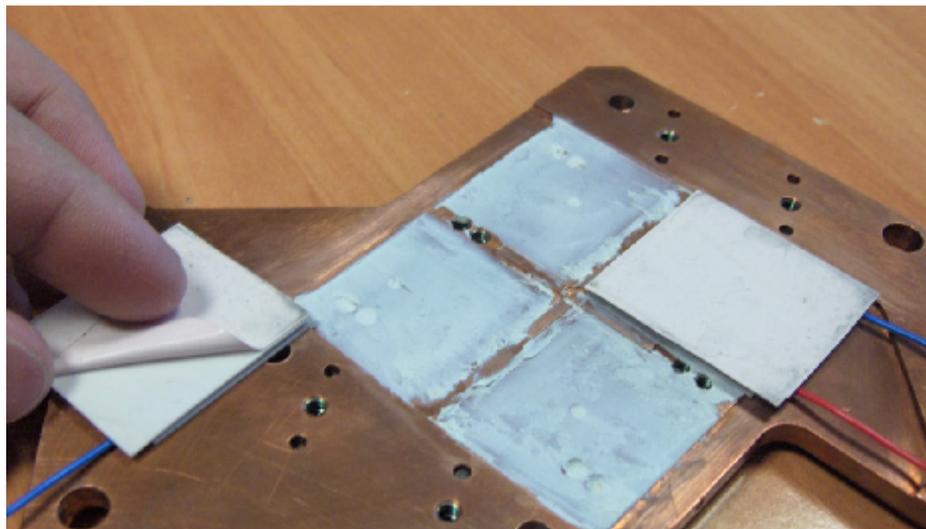
Figure 2.12 Pressure Sensitive Thermal Pad on the TEC Hot Surface

According to the TEC guidance handbook [33], if it is necessary to use more than one TEC module at the same location, the height variation between the modules should not exceed 0.025 mm. Lapped TEC modules have high surface quality therefore, all of the 4 TEC modules have been selected as lapped module with the most accurate surface tolerances for the assembly. After this process, the heat sink surface has been prepared. The preassembled TEC module has been integrated as shown in Figure 2.13.
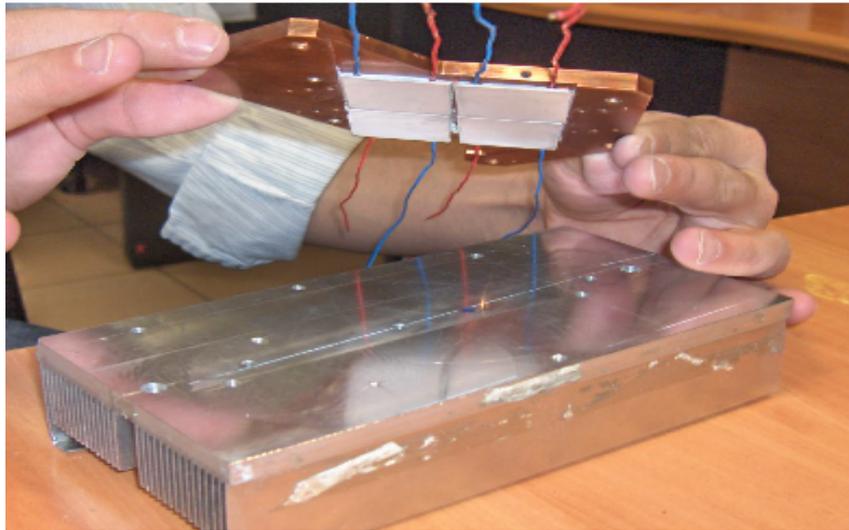
Figure 2.13 Base Plate and TEC Module Integrated with Heat Sink

Before fastening the module, screw elements should also be selected and prepared in order to maintain the most efficient mechanical and thermal configuration. As indicated in Figure 2.14, the screw element is not directly integrated to the system. A Belleville washer is used to absorb the additional torque loads during clamping and prevent TEC modules from breaking. The insulating fiber washer prevents assembly from thermal short circuit.
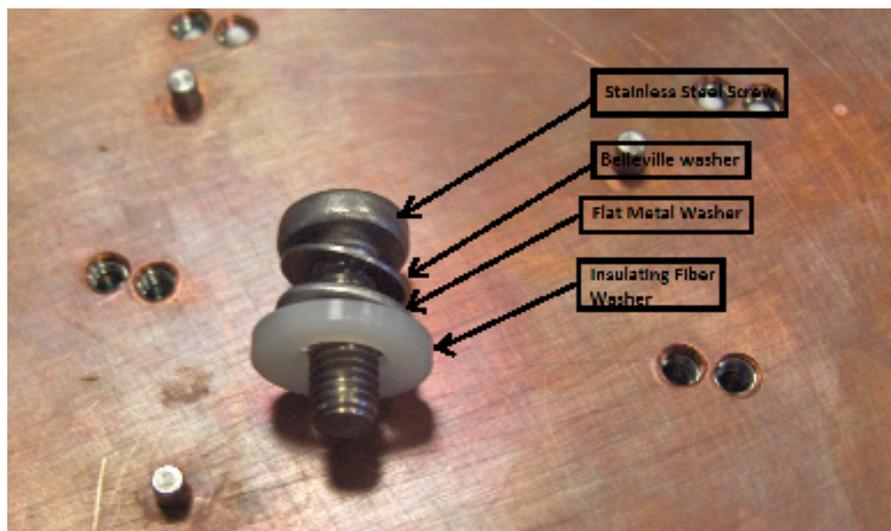
Figure 2.14 Screw and Washer System for the TEC Integration

According to the assembly guide four or five screws are recommended for a 4 TEC module [34]. If five screws are selected, one screw should be bolted from the center point firstly and the other four screws should be bolted from diagonal positions as crossing the centerline of the module. In this work, four screws have been used as in Figure 2.15.

Figure 2.15 The Assembled Base Plate, TEC Module and Heat sink

Since thermal interface materials and TEC module are very sensitive to mechanical effects, pressure load calculation has been performed before bolting. The recommended pressure load for ceramic structure TEC are from 1000 kPa to 2500 kPa [34]. The torque value applied to each screw during bolting can be calculated using the pressure load as shown below

$$T = (CxDxPxA)/(\#\ of\ screws) \tag{2.12}$$

T: Torque per screw (Nm)

C: Torque coefficient (0.20, 0.15 if lubricated)

D: Nominal screw size (M4 screw: ~ 4.00 mm)

P: Compression Pressure (N/mm^2)

A: Module surface area (mm^2)

To ensure a good thermal interface, there should be no bowing of either surface due to the applied torque. To prevent bowing, less torque should be applied if one or both surfaces are thinner than 3.2 mm for copper or 6.3 mm for aluminum [35].

An electrical impedance method is used to monitor the efficiency of the TEC module in every stage. An impedance meter device is used for this purpose by driving alternating current trough the device. Thus, the process is called as alternating current resistance (ACR) measurement [33]. Before and after the assembly, the impedance data are collected from electrically 4 series or 2 series x 2 parallel TEC module. 3-5 % deviation in the ACR value is considered to be significant change that can deteriorate the TEC performance. Some ACR data are provided in the Table 2.2;

Table 2.2 ACR Measurements of TEC Devices in Different Stages

Single TEC Module ACR Value (Ω)		
Before Assembly	After Mounting Cold Plate	After Fastening Screws at 1.2 Nm
Z_1= 1.17 Ω	Z_1= 1.21 Ω	Z_1= 1.19 Ω
Z_2= 1.19 Ω	Z_2= 1.21 Ω	Z_2= 1.20 Ω
Z_3= 1.19 Ω	Z_3= 1.19 Ω	Z_3= 1.20 Ω
Z_4= 1.20 Ω	Z_4= 1.22 Ω	Z_4= 1.22 Ω

These data are found to be acceptable for the TEC module. Hence, system may be assembled with the diode holder components.

CHAPTER 3

EXPERIMENTAL STUDIES ON THE LASER PUMPING CHAMBER

As it is mentioned previously, the main sources of the heat are the laser diodes and laser crystal.

- During the operation the net average heat load on laser crystal is
    5.2 W for 20 Hz pulsed mode.
- The remaining heat load on diode mounting components is
    30.8 W for 20 Hz pulsed mode.

Before manufacturing the laser pumping chamber and the final heat sink for the POD system, a preliminary experimental study has been performed. The aims of these preliminary experiments are,

- to simulate the operational conditions of the diode pumped laser device in laboratory conditions,
- to observe the thermoelectrically cooled laser heat generating model performance,
- to get feedback to design the final TEC module and heat sink configuration.

3.1 Construction of Laser Source Experimental Set Up

Since the heat generated in the laser components is already estimated, it may be simulated by electrical resistance elements mounted on diode holders as in Figure 3.1. The laser crystal heat load is added to diode holders and totally 36 W of heat load is tried to be removed with available heat sink – fan combination.
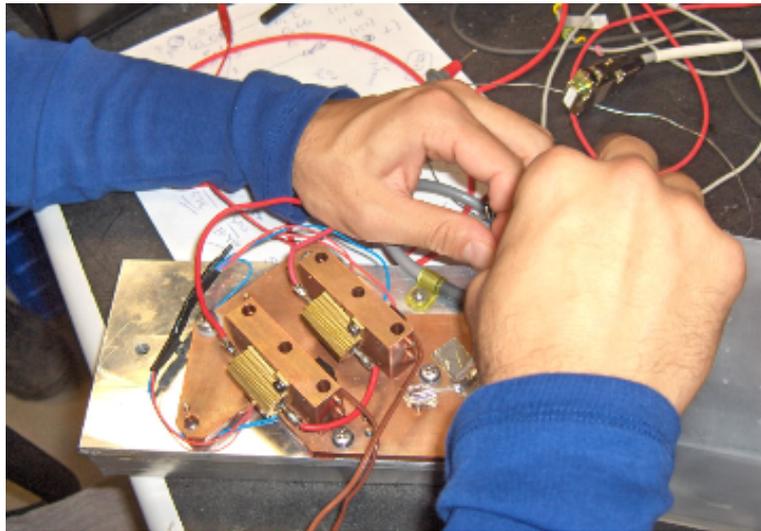
Figure 3.1 Mounted Electrical Resistances on Diode Pump Holders

Firstly, preassembled 4 TEC module is connected in electrically series configuration (4S) and ACR measurement yielded $Z_{tot} = 4.85\ \Omega$. After that, 4 series ACR value will be used to find out the TEC performance on the system.
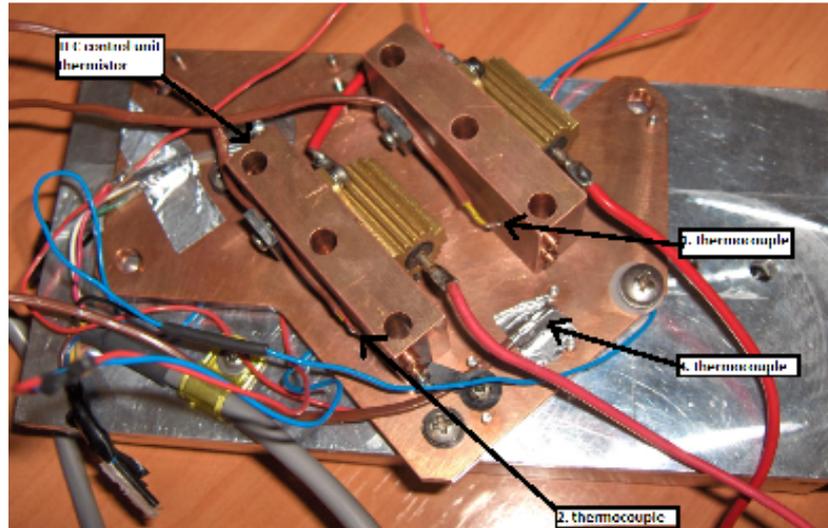
Figure 3.2 Thermocouple Locations on the Laser Source

After completing the electrical connections on the TEC control unit, the temperature measurement points are determined according to the system operational requirements. As it can be seen from Figure 3.2, there are three thermocouples. The first and the third thermocouples are fixed on the diode holders in order to find out the diodes temperature. The second thermocouple is mounted through a hole on the hot plate but its sensor region is in contact with the upper surface of the heat sink. The second thermocouple is used to measure the temperature of the TEC hot surface.

The thermistor is directly connected with the base plate and supplies temperature data to TEC control unit. The feedback temperature is used to regulate the TEC current value and direction to maintain desired temperature.

The system is enclosed with two plastic housings integrated to the system one by one as shown in Figure 3.3 and Figure 3.4.
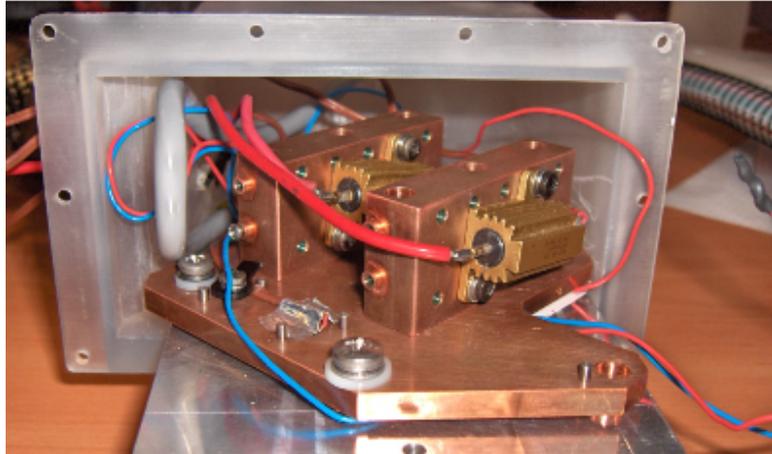
Figure 3.3 The Half of the Enclosure of the System

Figure 3.4 Completely Sealed Laser Source

In these experiments, four controllable electronic devices, fan controller, temperature measurement device, TEC module control device and electrical input power device are actively used as shown in Figure 3.5. In addition, desired ambient temperature is maintained with a large furnace.
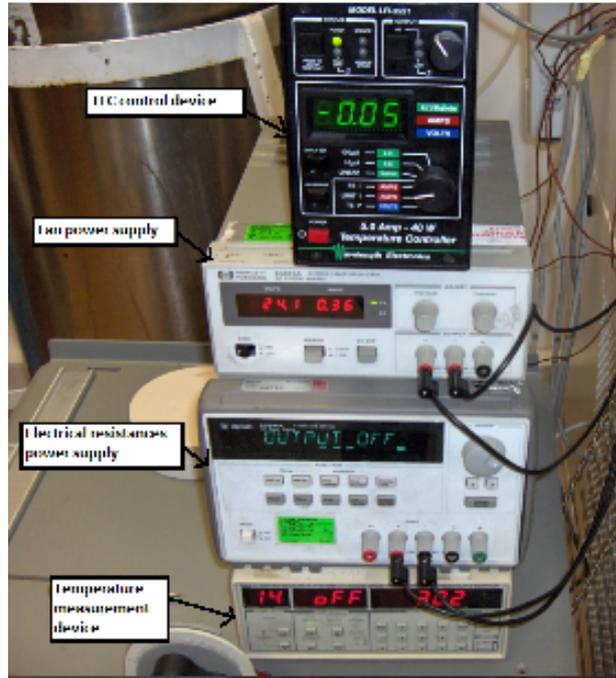
Figure 3.5 Electronic Controller, Power and Measurement Devices

The air cooled heat sink fan combination is formed in the furnace by considering the fan operating curve. One can see two additional thermocouples attached to the fin side in Figure 3.6. These thermocouples are used to measure the heat sink temperatures. One of them is located at the middle and deep region of the fins, the other is located at outer region of the fins. The necessary cable connections are made with a quick release apparatus, and attention was paid to disturb the air flow and temperature distribution.
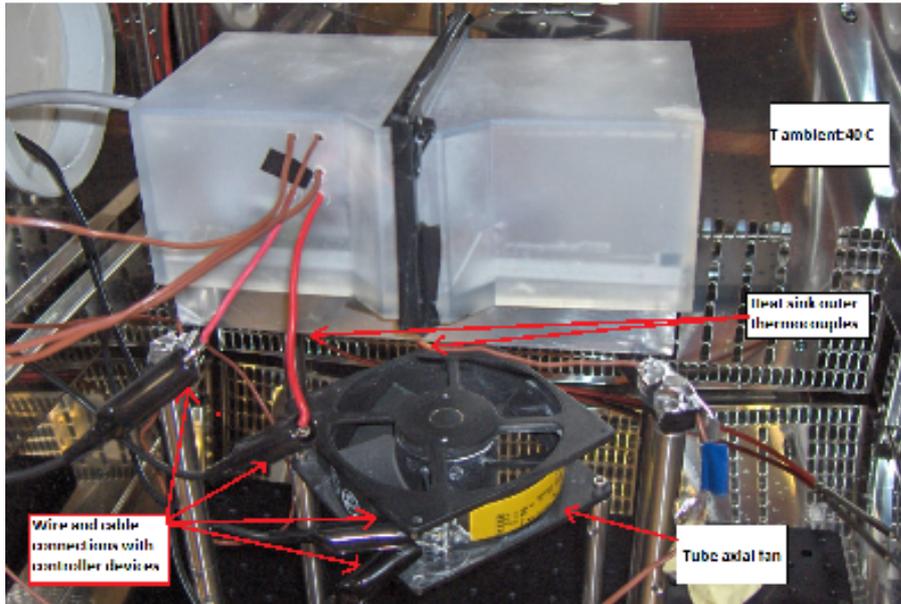
Figure 3.6 Complete Heat Sink and Fan Configuration inside the Furnace

The laser pumping chamber and the heat sink assembly is put in to the furnace, shown in Figure 3.7.

Figure 3.7 The Whole Experiment Set Up

3.2 Pumping Chamber and Heat Sink Experiments

3.2.1 The Method of Pumping Chamber and Heat Sink Experiments

In these experiments, four main parameters are controlled and observed their effects on the systems are observed:

- T_{amb} (Ambient temperature, maintained with the furnace)
- P_e (Heat load on the electrical resistances, controlled with the power supply)
- V_{fan} or V_{flow} (Air flow rate, controlled with the power supply)
- R_{set} or T_{set} (Resistance temperature value, maintained with the TEC module controller)

During the experiments, the main parameters are changed one by one and the resulting temperatures data are collected from thermocouple joints. Some other affecting parameters such as the electrical connection of wires and the insulation condition of the assembly are also investigated.

The main output data are:

- $R_{measured}$ or $T_{measured}$ (Value of set temperature, obtained from TEC controller)
- I_{TEC} (TEC module current value, obtained from the TEC controller)
- V_{TEC} (TEC module voltage value, obtained from the TEC controller)
- P_{TEC} (TEC module driving power, obtained from the I_{TEC} and V_{TEC})

The temperature measurement points are:

T_{15} = T_{diode1} (Temperature of diode holder 1)

T_{14} = T_{diode2} (Temperature of diode holder 2)

T_{13} = $T_{hot\_base\_plate}$ (Temperature of the base plate that is used to estimate T_c of the TECs)

T_{12} = $T_{top\_of\_heatsink}$ (Temperature of the top of the heat sink that is used to estimate T_h of the TECs)

T_{11} = $T_{heatsink\_fin1}$ (Temperature of the deeper region of the heat sink)

T_{10} = $T_{heatsink\_fin2}$ (Temperature of the outer and below side of the heat sink)

3.2.2 The Experimental Results

The experimental data have been taken with four TECs connected electrically in series. The ambient temperature is 40°C and a 6 W heat load was applied to the diode holders. 3.4 m^3 / min air flow rate was provided. The temperature control of TEC devices is realized by inserting thermistor tip on the base plate. The temperature value is set to 44°C based on the selected thermistor resistance. The set temperature of thermistor was chosen 44°C because diode holder temperatures becomes around 50°C, if the base plate is at around 44°C.

Table 3.1 Input and Output Data for Experiment #1

Experiment #1	4 electrically series TECs (4S TEC)					
Input Data	T_{amb} (°C)	P_e (W)	V_{fan} (V)	V_{flow} (m^3 / min)	R_{set} (Ω)	T_{set} (°C)
	40	36	28	3.4	4.5	44

Output Data	$R_{measured}$ (Ω)	$T_{measured}$ (°C)	I_{TEC} (A)	V_{TEC} (V)	P_{TEC} (W)	T_{15} (°C)	T_{14} (°C)	T_{13} (°C)	T_{12} (°C)	T_{11} (°C)	T_{10} (°C)
	4.5	44	1.17	8.7	10.2	49.2	51.1	45.1	45.2	44.5	43.7

Output data are collected after waiting for 20 minutes beyond which a steady state condition is assumed to hold. It is seen that temperature of the diode holders is kept around 50°C. The temperature difference between two diode holders arise from the thermal resistance difference of the diode holders. Two holders may have different surface tolerances as a result different contact resistance values obtained. Besides that, diode holder that faced with the lower performance TEC can be less cooled. In the theory, if one obeys all the assembling tips and rules, 4 TEC modules should perform same performance. However, if the common base plate is tilted during integration or thermal interface material applied at any different thicknesses; cause TEC modules to show different characteristics.

The input power to the TEC is 10.2 W which is in reasonable levels. It means that with the available heat sink-fan configuration, 36 W+10.2 W = 46.2 W is rejected to the ambient. The thermal resistance between the TEC module and the ambient may be calculated as follows

$$\Delta T_{TEC-Ambient} = Q \times R_{TEC-Ambient}$$

(3.1)

$$R_{TEC-Ambient} = \frac{\Delta T_{TEC-Ambient}}{Q}$$

If the average temperature of the hot side of the TEC module is taken as 47°C near but higher than T_{12} ;

$$\Delta T = 47 - 40 = 7\,°C$$

(3.2)

$$Q = 46.2\ W$$

(3.3)

$$R_{TEC-Ambient} = \frac{\Delta T}{Q} = \frac{7}{46.2} = 0.15\,°C/W$$

(3.4)

The C.O.P value for the TEC module may be calculated as

$$C.O.P = \frac{Q_C}{P_{TEC}} = \frac{P_e}{P_{TEC}} = \frac{36}{10.2} = 3.52$$

(3.5)

which is within the ideal operational range of the TEC.

3.2.3 Observations from the Experiments

After completing eight additional experiments, the following observations were made which have been utilized for the final TEC embedded laser pumping chamber design for the POD application.

- The performance of the TEC module is easily affected by the ambient temperature, the applied heat load, T_c, T_h and ambient thermal resistance parameters. During the design stage all these parameters should be well defined.
- While TEC module can withstand challenging inputs, the input power of the TEC module always increases. This means extra heat load should be removed from the hot side of TEC module.
- TEC module shows consistent performance with the manufacturer product performance graph. This simplifies the selection and the design procedures of TEC systems.
- The electrical connection of the TEC module does not change the cooling performance. This provides easier supply of the TEC input power.
- Since any type of thermal resistance deteriorate the cooling efficiency of the TEC, one should avoid from any wrong operation or process or material causing thermal resistance.
- TEC modules can give quick response to changing environment conditions. This makes the TEC modules reliable.
- Since the TEC modules are tunable, it is beneficial to operate the module with a closed loop temperature control.

3.3 Comparing Experimental and Software Analysis Results

Parallel to the experimental studies, a software model with same configuration is formed and driven at IcePak program as shown in the Figure 3.8.
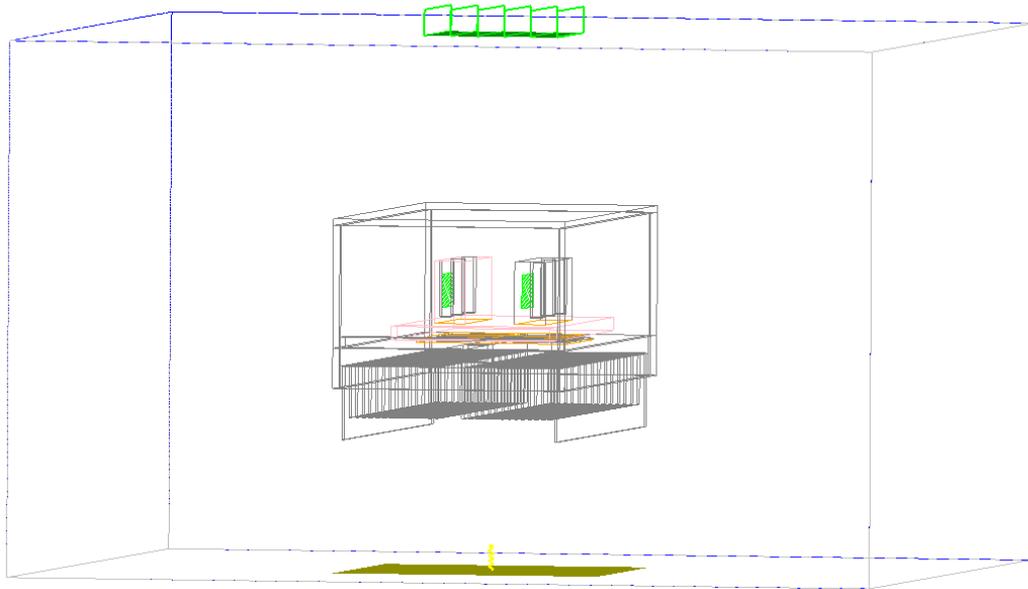
Figure 3.8 The Heat Sink – Fan System Model in Software Analysis

System modeling is done by considering component dimensions, material properties and boundary conditions. Heat generation on the resistances is simulated by defining heat flux on diode holders with the same resistance cross-sectional area. The fan is simulated by defining the air flow rate at the same location with respect to the heat sink as in the experiments. Control volume dimensions are also specified according to the experimental control volume.

After obtaining the experimental results, they are compared with the CFD simulations. The thermal impedance values are given in Table 3.2.

Table 3.2 Present and Selected Materials Impedance Values

Contact Thermal Resistance Region	Thermal Impedance $(m^2 K / W)$	Expected Thermal Impedance $(m^2 K / W)$
Cu-Cu	1.200e-04	9.00e-05
Cu-AlO (T_c side)	9.00e-05	2.00e-05
AlO-Al (T_h side)	9.00e-05	2.00e-05

Since the copper diodes and the base mounting plate should be precisely machined, Cu-Cu thermal impedance should match the expected thermal impedance value shown in Table 3.2. Between copper and the ceramic surfaces of the TEC (both cold and hot sides), a graphite based thermal interface material produced by eGraph Inc. is used. This material has superior thermal properties compared with the available thermal pad. In Table 3.3, thermal property and impedance values are given for graphite based materials.

Table 3.3 Thermal Properties of eGraph 1200 series Thermal Pad Materials [36]

Typical Properties of eGraf 1200 Materials

Property	eGraf 1205	eGraf 1210	eGraf 1220	Test Method
Physical				
Color	Dark Grey	Dark Grey	Dark Grey	
Thickness	0.13 mm	0.25 mm	0.51 mm	
Tensile Strength	1800 kPa	3100 kPa	3100 kPa	ASTM F-152
Thermal				
Operating Temperature	-40 to 400 °C	-40 to 400 °C	-40 to 400 °C	
Thermal Impedance @100 kPa	0.32 cm²°C/W	0.54 cm²°C/W	0.98 cm²°C/W	ASTM D 5470 Modified
Thermal Impedance @700 kPa	0.10 cm²°C/W	0.27 cm²°C/W	0.56 cm²°C/W	ASTM D 5470 Modified
Thermal Conductivity				
Thru-thickness	10 W/m•K	10 W/m•K	10 W/m•K	ASTM D 5470 Modified
In-plane	120 W/m•K	120 W/m•K	120 W/m•K	Angstom's Method

In the laser pumping chamber of the POD system, the materials eGraph 1205 and 1210 have been used which showed lower thermal impedance performance at the compressing pressure values of the system.

CHAPTER 4

· CONSTRUCTING THE HEAT SINK OF THE POD LASER CHAMBER

In laboratory conditions, a TEC module of four thermally parallel, electrically series TECs provided sufficient cooling to the laser source. It has been observed that the TEC module performance is very much affected from environmental conditions. In order to achieve the required cooling in the POD application, proper mounting of the base plate, the diode and the crystal holder, thermal interface pad, heat sink design and thermal resistance value should be determined.

4.1 Final Heat Sink Model Analysis

Based on the literature survey [37] and several iterations with the CFD (Fluent) analysis, a bow shape plain finned heat sink model as shown in Figure 4.1, has been formed in order to meet the cooling and air flow requirements in the specified POD inner volume.
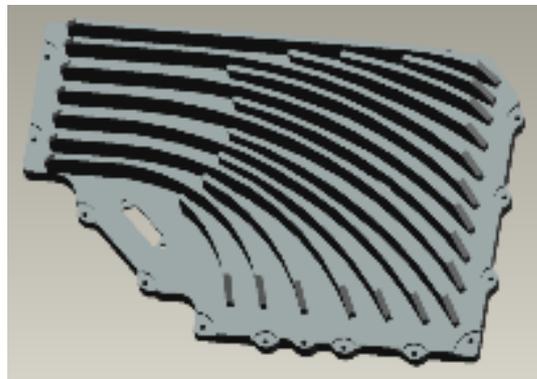
Figure 4.1 New Bow Shape Plain Finned Heat Sink

The fins are curved over the heat generating region in order to direct the air flow to the hot spot. The same height of the fins does not influence the air flowing characteristic and the interaction between air and base of the fin surfaces are also supplied.

A housing component (lid) of the laser device is also designed and the control volume of the laser device can be simulated as in the actual case. The assembled form of housing and heat sink are shown in Figure 4.2.
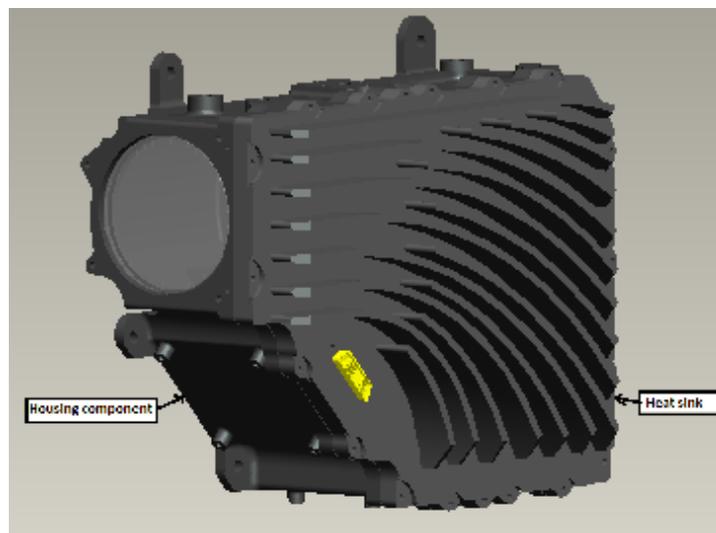
Figure 4.2 Closed Assembly of Laser Device

At this stage, it has been decided to perform the CFD analysis as in the actual case. The POD envelope and other POD assembly device models are also created as in actual case and embedded into Fluent CFD program.
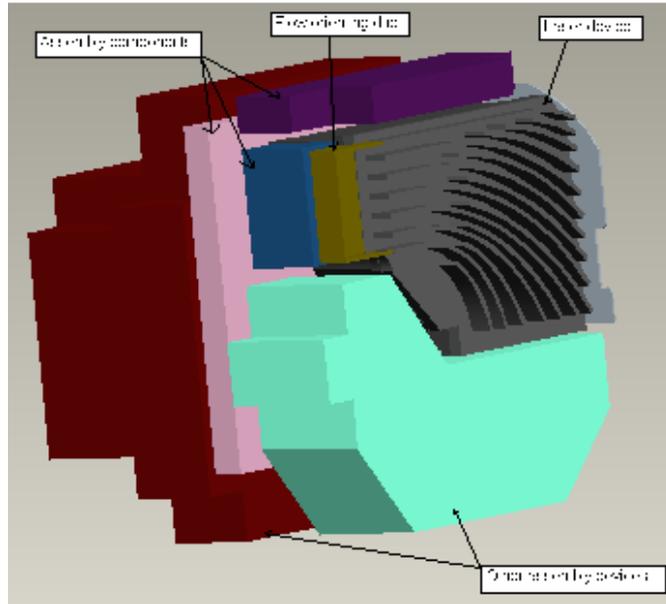
Figure 4.3 Pod Assembly Components

Since the cooling and air flow duct configuration of the POD is known, the duct components are also created and integrated with the POD envelope as in Figure 4.4.
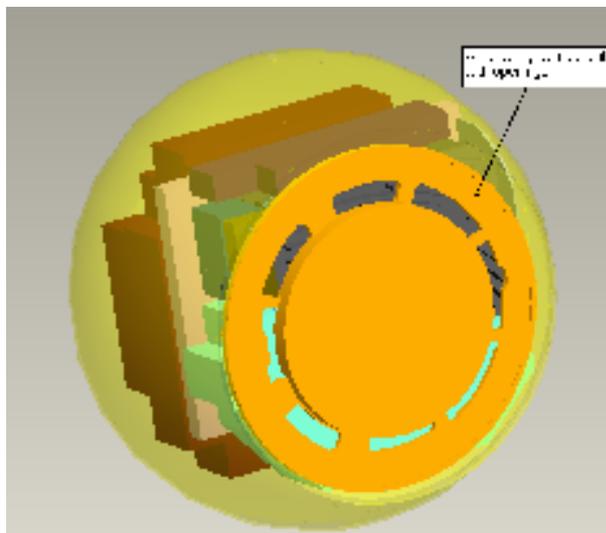
Figure 4.4 Assembly with the Air Inlet Component

As it is seen in Figure 4.4, air enters the system from the openings of the yellow part. The air flow is supplied to the yellow part from the wing component shown in Figure 4.5;
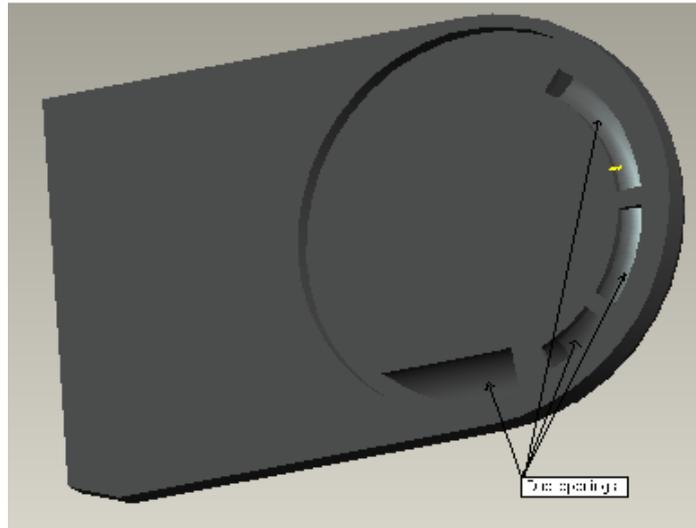
Figure 4.5 The Duct Component and its Openings

The air flow duct component has four openings which provide the air flow into the POD housing. This part is then assembled to the outer enclosure and the system is fully closed as the in Figure 4.6.
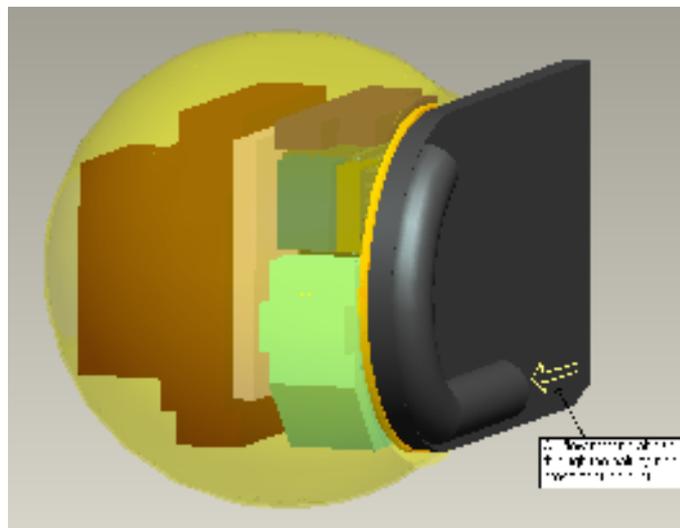
Figure 4.6 The Completed Assembly Model

After creating three dimensional models, several analyses have been performed with FLUENT CFD program.

Air flow of 2.3 m^3/min at 32°C is supplied to the POD system as shown in Figure 4.6. Different heat sink materials have been tested. The ambient temperature was taken as 40°C. The total applied heat load was equal to 60 W over the surface area of the TEC module.

First, a transient analysis of aluminum heat sink model has been completed. The resultant velocity profile in the POD enclosure and heat sink fins is shown in Figure 4.7.
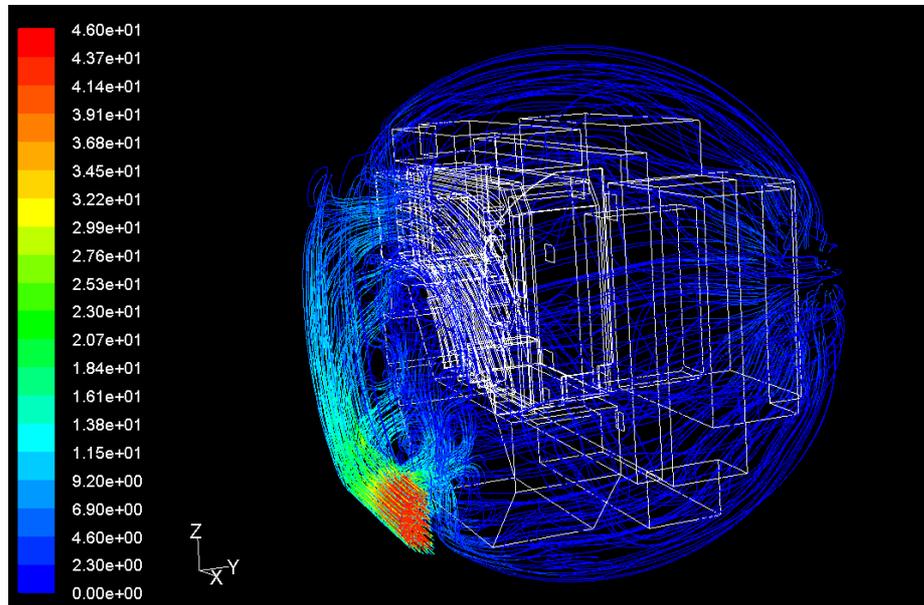
Figure 4.7 Velocity Profile in the Pod Enclosure

It may be observed that the maximum velocity occurs at the entrance location which has the smallest cross sectional area and causing the highest pressure drop. The velocity profile indicates that the flow velocity decreases at the exit area.
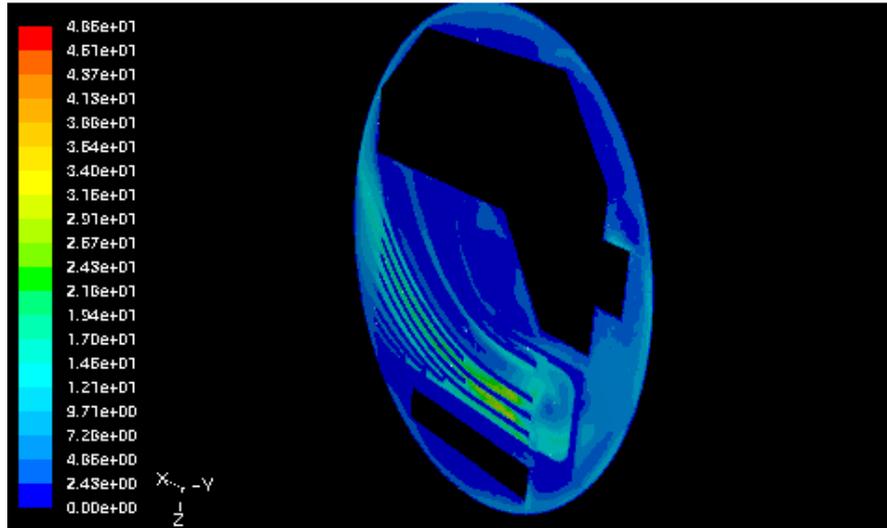
Figure 4.8 Velocity Profile at the Heat sink Fin Surface

From Figure 4.8, it may be seen that the orienting duct has critical effect on the air flow of the system. The air flow can be directed to the hot spot region through the fin passages that increase convective heat transfer coefficient around the hot spot. The temperature distribution on the aluminum heat sink may be seen in Figure 4.9.
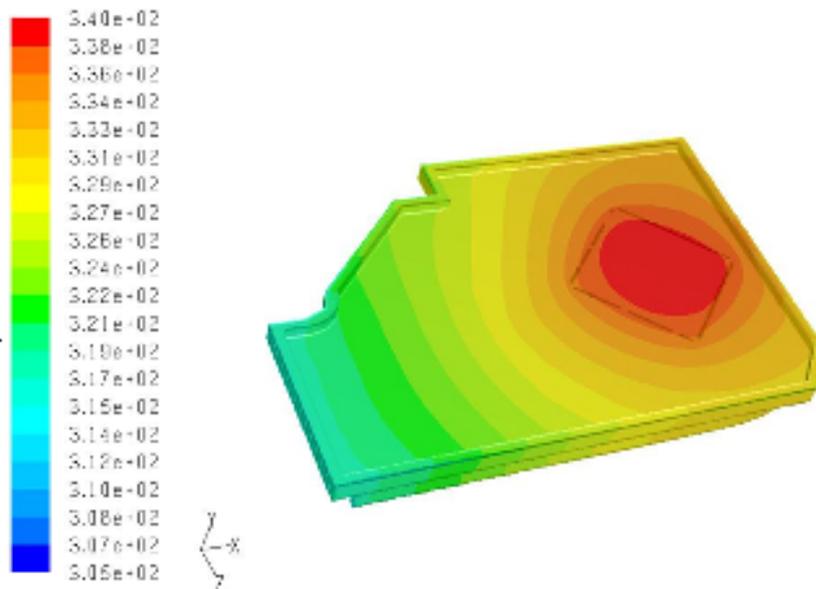
Figure 4.9 Temperature Profile of the Aluminum Heat Sink after 400 s

As may be seen in Figure 4.9 the hot spot is localized and reaches a maximum temperature of 340 K (67°C). Hence, the hot region should be enlarged and its average temperature should be decreased. The variation of the average aluminum heat sink temperature is presented in Figure 4.10.
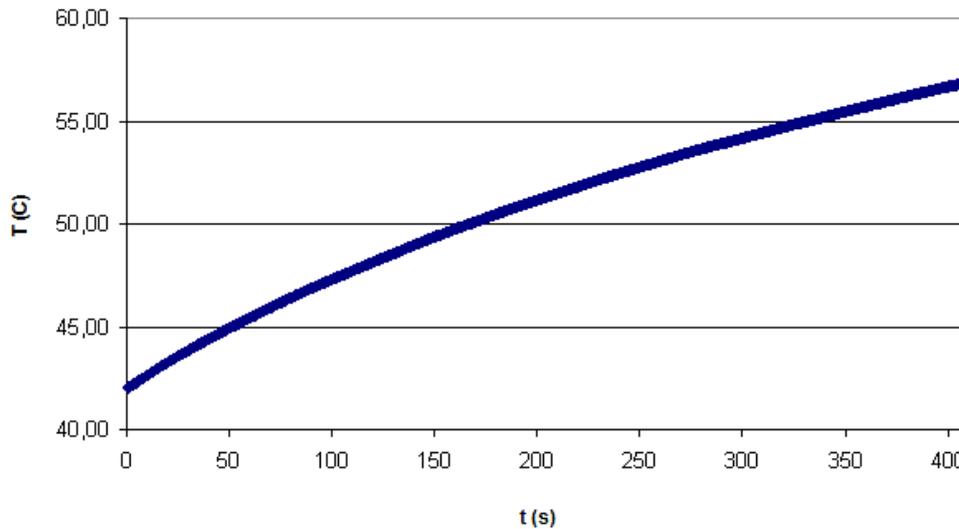
Figure 4.10 Variation of the Average Aluminum Heat Sink Temperature

After the tests with aluminum, a copper heat sink model has been tested with the same inputs and boundary conditions. Better results have been obtained in terms of the temperature profile as shown in Figure 4.11. The velocity profile did not change because of the same heat sink and duct geometries. One disadvantage of copper heat sink is that, it is heavier than aluminum.
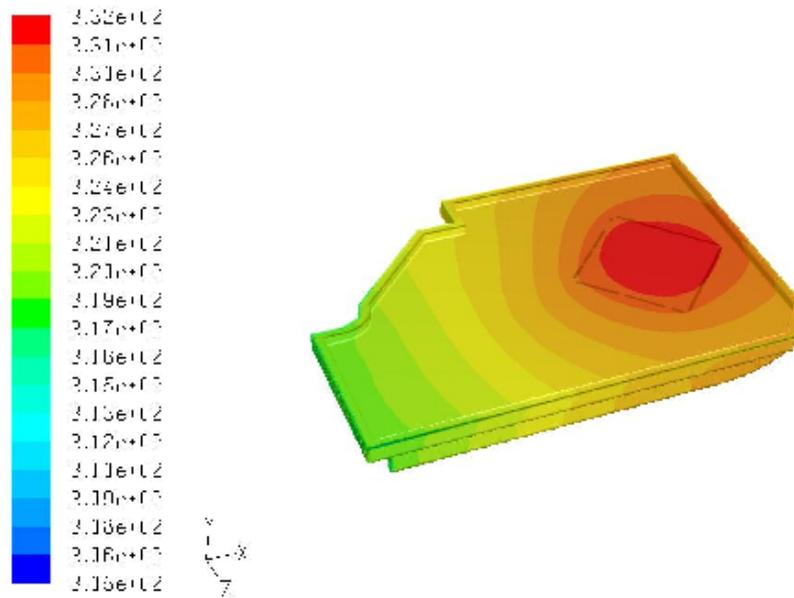
Figure 4.11 Temperature Profile of Copper Heat Sink after 400 s

It is seen that temperature improvement is obtained with copper material. The hot spot region is larger than aluminum which means more homogeneous temperature distribution is obtained. The maximum temperature is 332 K (59°C) which has 8°C lower than aluminum one. The variation of the average copper heat sink temperature is presented in Figure 4.12
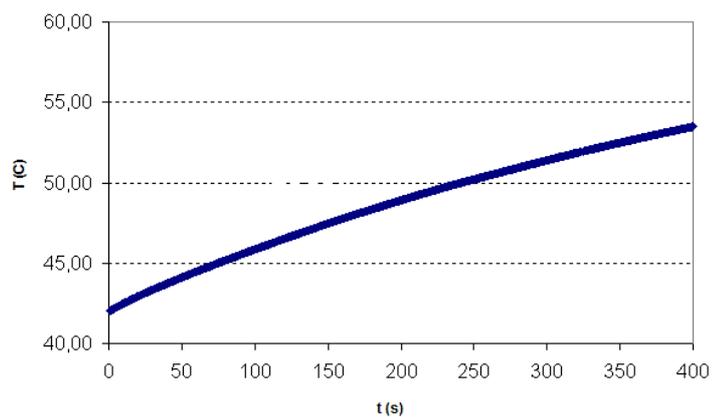
Figure 4.12 Variation of the Average Copper Heat Sink Temperature

According to the TEC performance curve and the experimental data, the maximum hot side surface temperature of the TEC should be 60-65°C in order to obtain high TEC efficiency for these selected TECs. This means that copper heat sink model satisfies the cooling requirement with a maximum TEC hot side temperature of 59°C.

CHAPTER 5

EXPERIMENTAL STUDIES ON THE LASER PUMPING CHAMBER WITH HEAT SINK IN POD SYSTEM

In Chapter 4, heat sink design of the laser pumping chamber is completed according to POD working conditions with the help of CFD (Fluent) analysis. POD is an airborne assembly consisting of different devices such as an infrared camera, receiver optical assembly, laser pointer and laser designating device. Stereolithography (SLA), rapid prototype, of the infrared camera, receiver optical assembly, laser pointer and other electrical components have been used for the POD experiments. On the other hand, for the laser device, actual laser pumping chamber, heat sink and housing lid have been used as mentioned previously.

5.1   Constructing POD Experimental Set Up

5.1.1   Constructing TEC Coupled Pumping Chamber with Heat Sink

First, the laser designating device has been constructed in the sequence of the assembly components. Before the other components, the TEC module is prepared to be integrated between the copper heat sink and the base plate. The used thermal interface is graphite based thermal pad, eGraph 1205, a product of Graftech Corporation. This thermal pad has been applied both cold and hot surfaces of the TEC module after the cleaning and degreasing processes.

Once the TEC modules are prepared as in Figure 5.1, they are gently placed on the already machined groove on the heat sink plate.
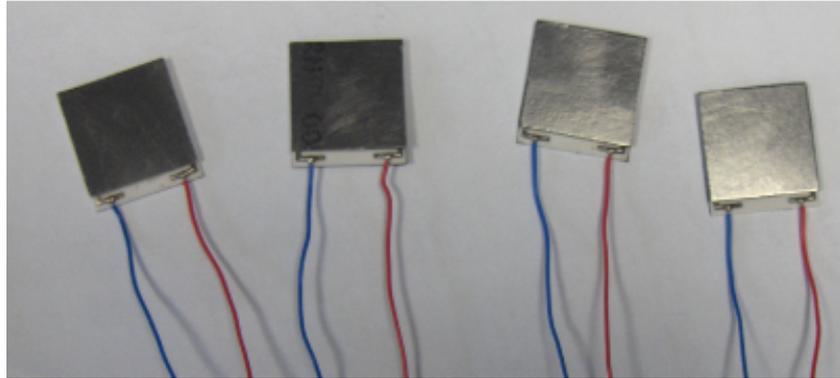
Figure 5.1 Adhesive Thermal Pad Applied on both Hot and Cold Sides of the four
TEC Modules

As it may be seen in Figure 5.2, hot side surfaces of the TEC modules are placed on
the rectangular groove on the heat sink together. As mentioned before the four high
precision surface plastic bosses are used to mount the base plate and prevent the
system from a thermal short circuit. The base plate made of copper material has been
mounted by applying sufficient amount of pressure on TEC surface and thermal
pads. The mounted base plate is shown in Figure 5.3.
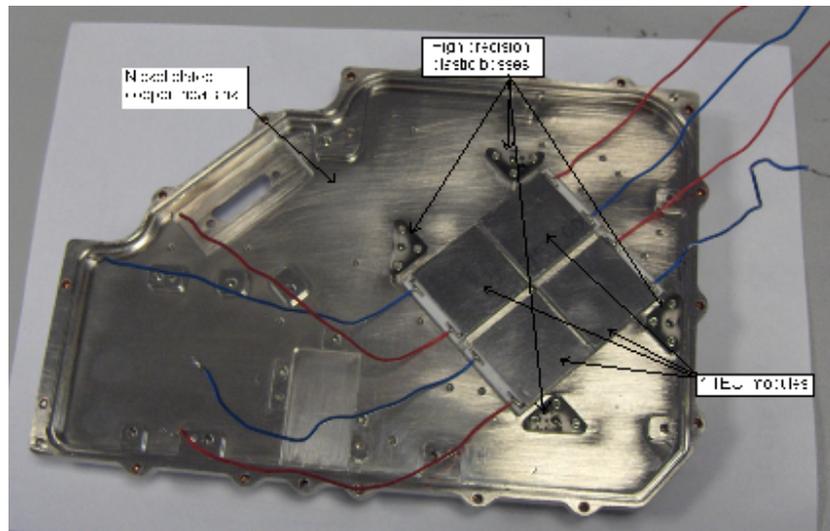
Figure 5.2 TEC Modules Placed on the Heat Sink
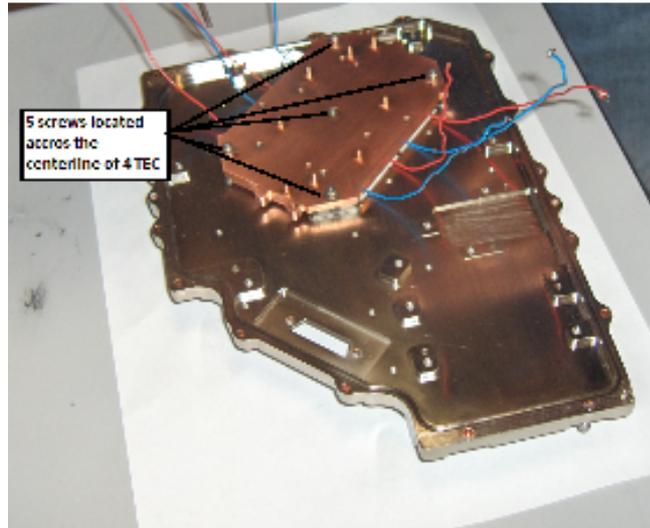
Figure 5.3 Mounted Copper Base Plate

According to the thermal pad compression recommendations, 2000 kPa pressure is implemented by five screws by applying 1.4 Nm torque to each screw [38]. After the base plate is mounted, as can be seen in Figure 5.4, two symmetrical diode holders have been assembled on the plate by copper to copper surface contact. The heat generating electrical resistances have also been mounted on the two diode holders in order to simulate the laser diodes. The TEC controller device has a function of closed loop temperature control using a thermistor on the required surface. Thermistor supplies a temperature feedback, and the controller drives the TEC module in the negative and positive directions.
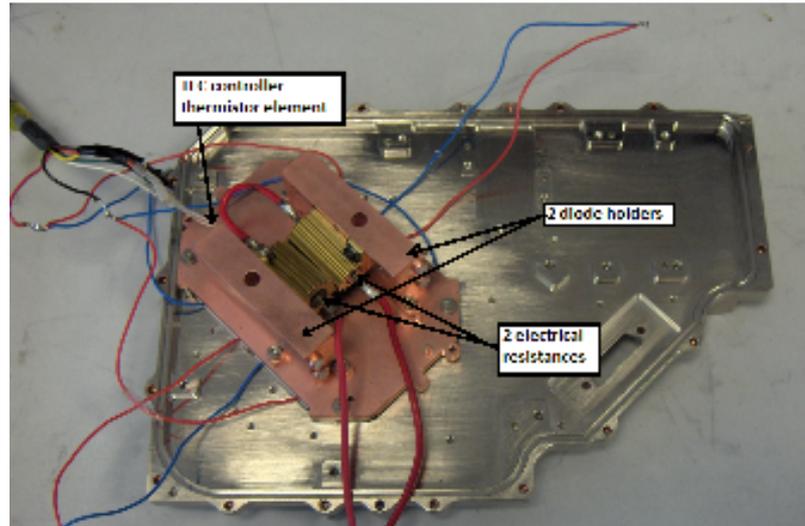
Figure 5.4 Diode Holders, Electrical Resistances and TEC Controller Assembled
System

Usually, TEC modules are operated in the negative direction in order to maintain the
diodes temperature at 50°C which is higher than the ambient temperature 40°C.
Negative direction means that the TEC module removes heat from the lower to the
upper direction to meet the diode temperature requirement while the diodes do not
generate heat. However, when they operate and heat generation occurs, the TEC
controller starts to operate the TEC module in the positive direction which means
that the TEC module removes heat from up to down.

During the experiments, in addition to the thermistor temperature data, some
thermocouples are also mounted on desired locations in order to take regular data
from the inner structure. Since the diode holders are the most critical temperature
control components, two thermocouples are inserted on the two holders. Another
thermocouple is mounted on the base plate and the other two thermocouples are fixed
on the upper surface of the copper heat sink. The thermocouple locations may be
seen in Figure 5.5.
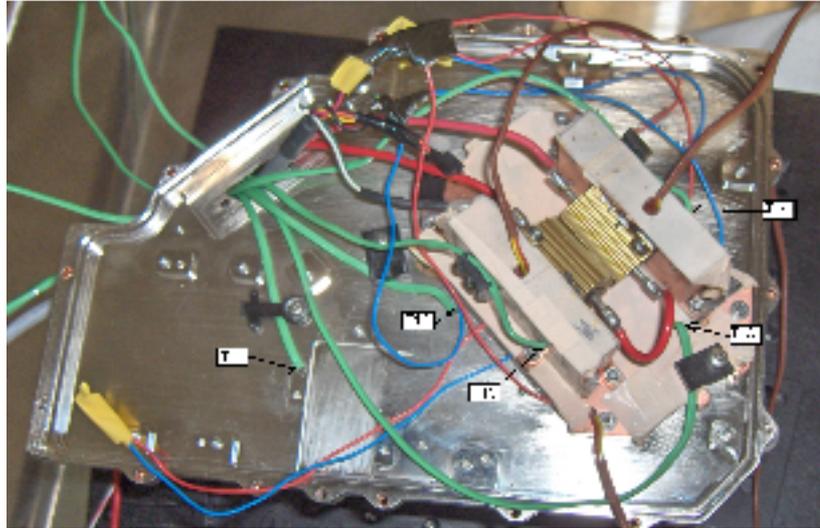
Figure 5.5 Temperature Measurement Thermocouples Locations

Temperature data is collected from five measurement points as indicated below

$T_{15} = T_{diode1}$ (Temperature of diode holder 1)

$T_{14} = T_{diode2}$ (Temperature of diode holder 2)

$T_{13} = T_{hot\_base\_plate}$ (Temperature of the base plate that is used to estimate T_c of the TECs)

$T_{12} = T_{top\_of\_heatsink1}$ (Temperature of top of the heat sink near the hot spot that is used to estimate T_h of the TECs)

$T_{11} = T_{top\_of\_heatsink2}$ (Temperature of far side of the heat sink from the hot spot)

$T_{10} = T_{air\_flow\_in\_duct}$ (Temperature of air stream pumped through the plastic duct)

Next, the aluminum housing component of the laser device has been assembled with the heat sink system. This component is the enclosure of the system and supplies sealing against the ambient effects. In Figure 5.6, the assembled system may be seen including the air orienting duct component. This part has a function of directing the air flow through the hot region of the heat sink.
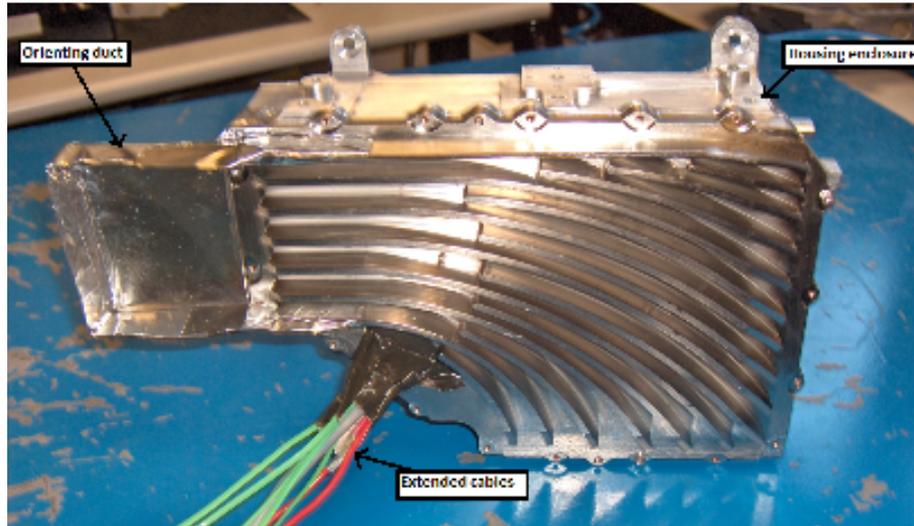
Figure 5.6 Fully Closed and Sealed Laser Assembly

The cables are extended to the outside for integration with the electrical power, measurement and controlling devices. The opening for the cables and is sealed using sealing tapes. Laser device experiment set up is completed and the outer POD assembly should be formed. The outer systems components have been manufactured by other departments. Some parts have been obtained from rapid prototype techniques for simulating the entire POD sensor suit.

5.1.2 Construction of the POD Assembly

The outer housing of the POD has a spherical geometry which has been manufactured by investment casting. It has some mechanical mounting details to carry the inner devices and also some openings to provide the cooling. In Figure 5.7, free pod outer housing may be seen with its details.
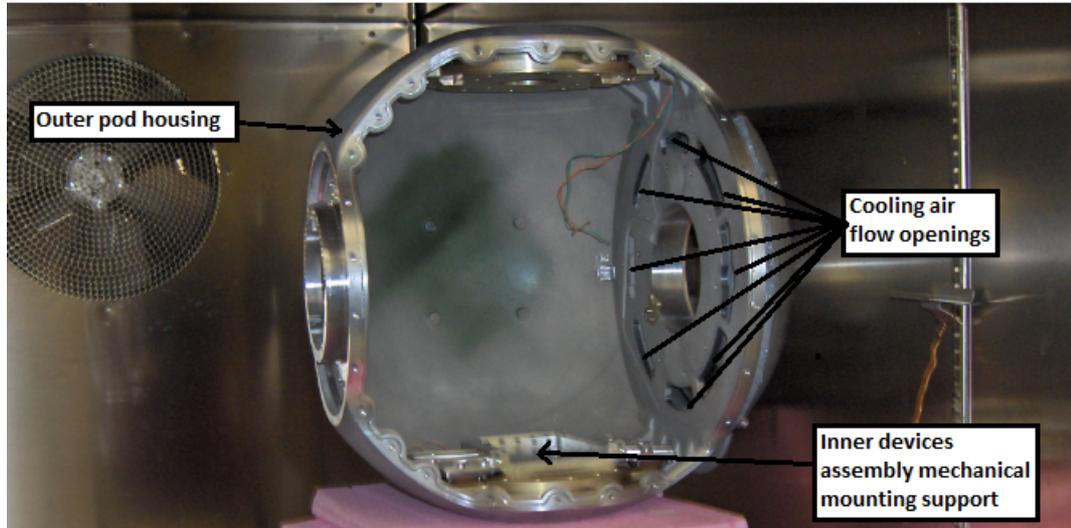
Figure 5.7 Geometric Details of Outer Pod Housing

The completed POD inner structure assembly can be seen in Figure 5.8.
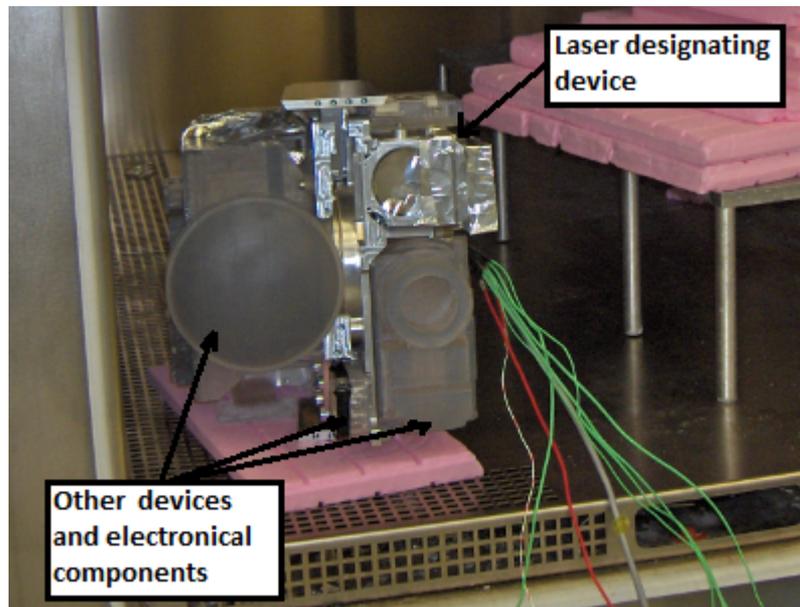
Figure 5.8 POD Inner Structure Assembly

Before the system construction, the cooling and ventilating model of the pod system should also be simulated. In the real application, POD inner volume is expected to be

maintained between 5 to 40°C by an additional environmental control unit (ECU). This unit will supply cooling air between 2.3 to 3.4 m^3 / min flow rates at 2 to 32°C.

For the experimental studies, the worst thermal conditions have been applied. During the experiments, the temperature of the ambient has been maintained by using furnace. The ECU is simulated by an alternative fan-duct cooling system made of plastic. This component may be seen in Figure 5.9 and Figure 5.10.
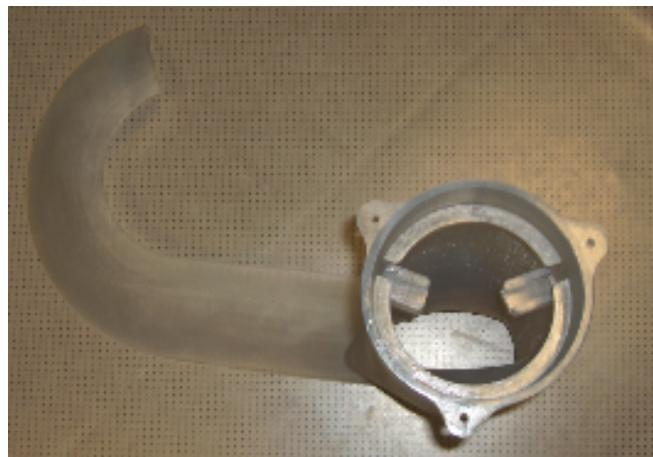
Figure 5.9 Top View of the Rapid Prototype of the Plastic Duct
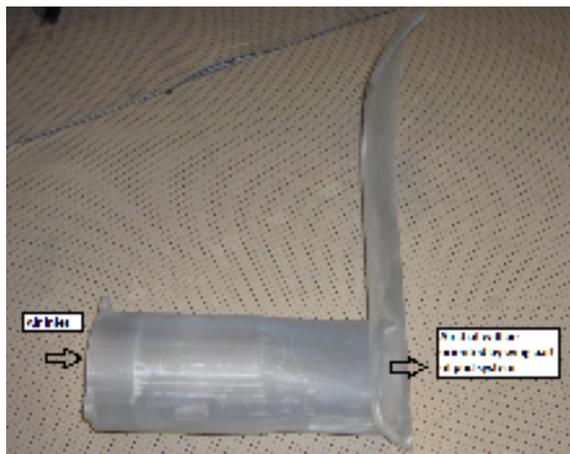
Figure 5.10 3-D View of the Rapid Prototype of Plastic Duct

This plastic component has a duct function when it is connected with the wing part of the POD system. The wing part provides the mechanical rotation to the POD housing

in addition to providing air flow from the duct. This wing part was modeled in the Chapter 4 with a geometry shown in Figure 5.11.
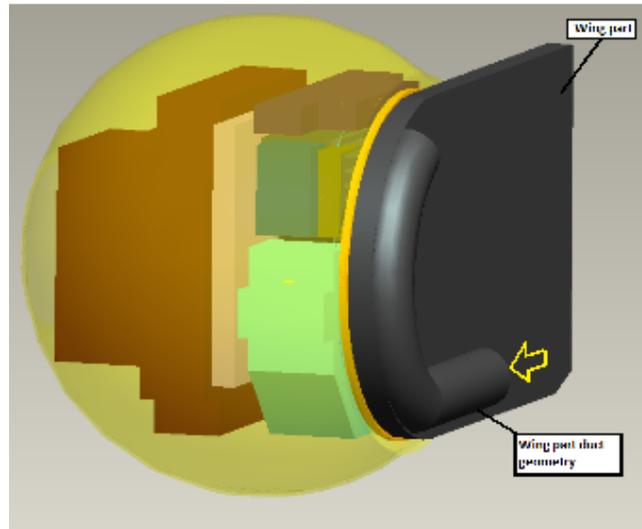
Figure 5.11 Modeled Wing Part Duct Geometry

In order to manufacture the most similar duct to that in the analysis, both of the plastic duct and the wing part have been integrated as in the real case shown in Figure 5.12. The integration has been done by bonding all the contact surfaces and fastening with several screws.
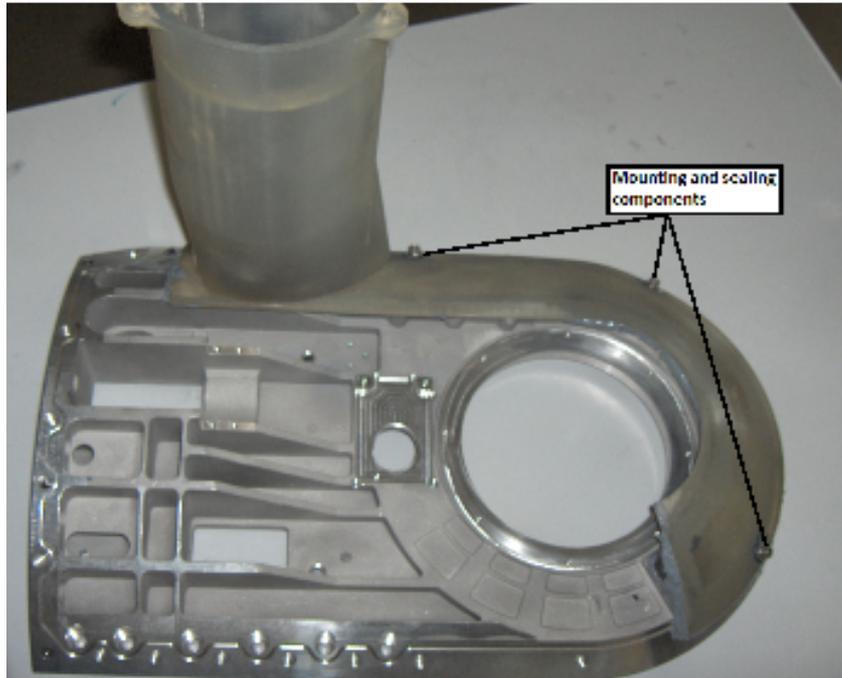
Figure 5.12 Bonded Assembly of the Plastic Duct on the Wing Part

The open side of the bonded assembly is shown in Figure 5.13.
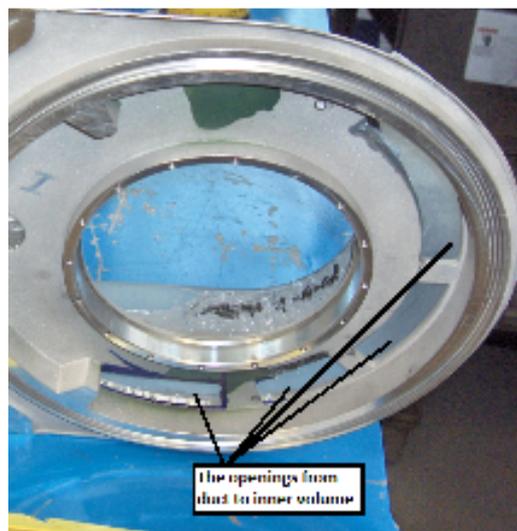
Figure 5.13 The Open Side of the Bonded Assembly

Completed air flow duct assembly is connected with the outer pod housing and positioned in the furnace as shown in Figure 5.14.
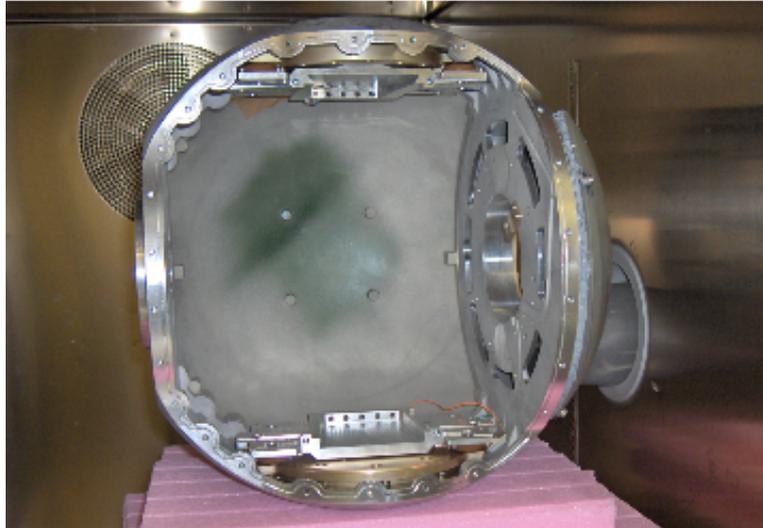
Figure 5.14 Assembled Pod Outer Housing with the Duct System

At this stage, because of the air flow and thermal requirements, a thermocouple, a heater and a tube axial fan have been inserted in the cylindrical extension of the plastic duct. As in Figure 5.15, firstly the thermocouple has been fixed by aluminum tape on the inner surface of the plastic duct in order to measure the temperature of the forced air inside the pod system. Then, a 90 V electrical heater is placed on the machined grooves of the plastic duct.

Figure 5.15 Mounted Thermocouple and Heater Component

After the thermocouple and the heater are fixed, a 115 V 400 Hz AC axial Ametek Rotron brand fan has been inserted and fastened using three screws by a lid component. The completed fan-heater assembly may be seen in Figure 5.16.
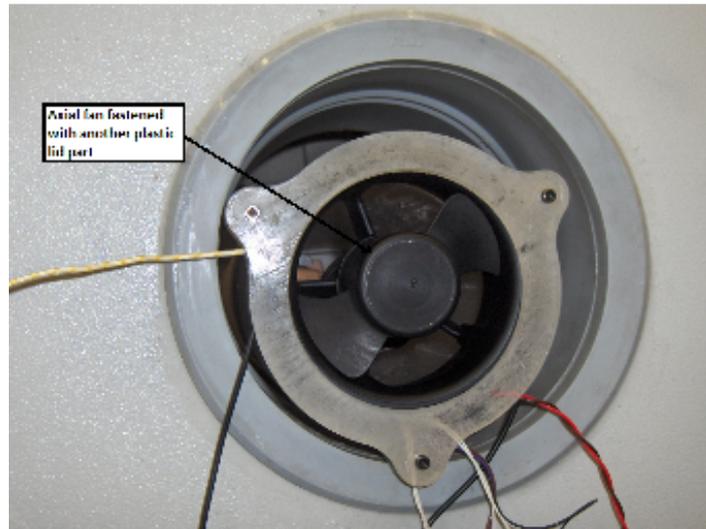
Figure 5.16 Completed Fan-Heater Assembly

This fan-heater configuration is constructed to force the heated ambient air into the furnace at the required flow rate. Since the environmental temperature is around 23 °C in the test room, the heater voltage is tuned until an inlet temperature of 32°C is achieved.

Next the inner structure assembly has been placed in the outer housing of the pod. In Figure 5.17, last stage of the set up may be seen before completely closed.
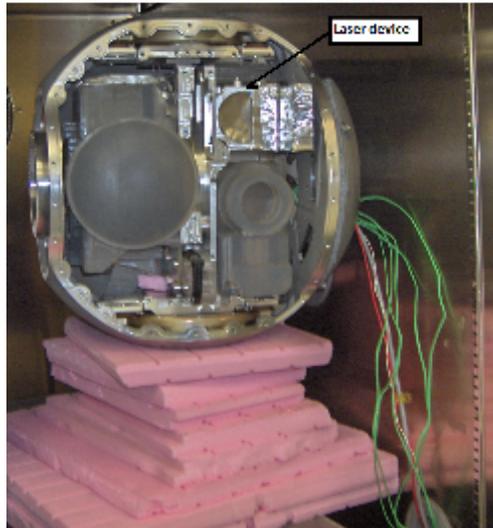
Figure 5.17 The Assembly of the Inner Structure and Outer Pod Housing

After checking the device positions once more, the big front lid has been closed. In Figure 5.18, the fully completed and sealed POD assembly may be seen.
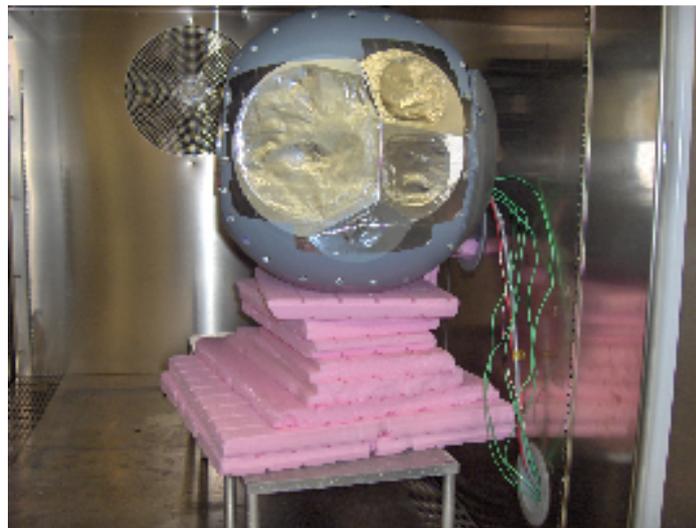
Figure 5.18 Completely Sealed and Closed Pod Assembly Set Up

The opening of the POD is maintained as in the real device geometry in Figure 5.19. The air flow rate generated by the fan is measured from this opening.
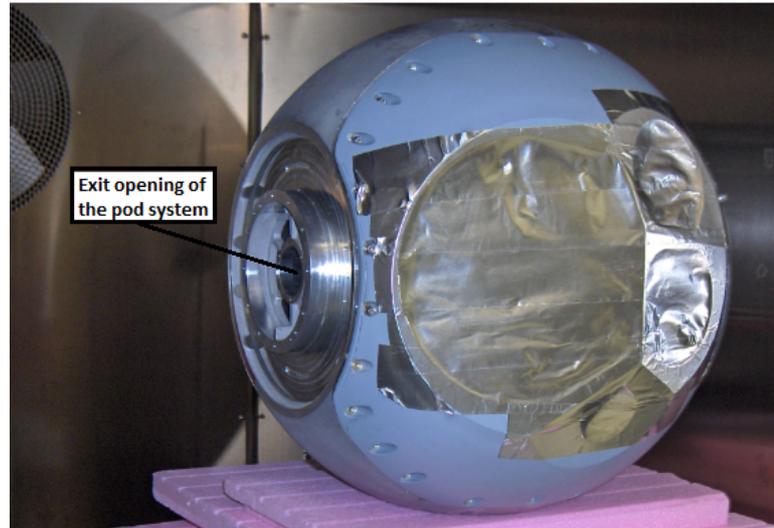
Figure 5.19 The Openings Left in the Pod Assembly

Afterwards, the big furnace has been sealed by closing its door and system became ready to operate after making the data and power connections. In Figure 5.20, the sealed pod assembly in the big furnace may be seen.

Figure 5.20 The Sealed Pod Assembly Set Up in the Furnace

The controller, power and data measurement devices may be seen in Figure 5.21.
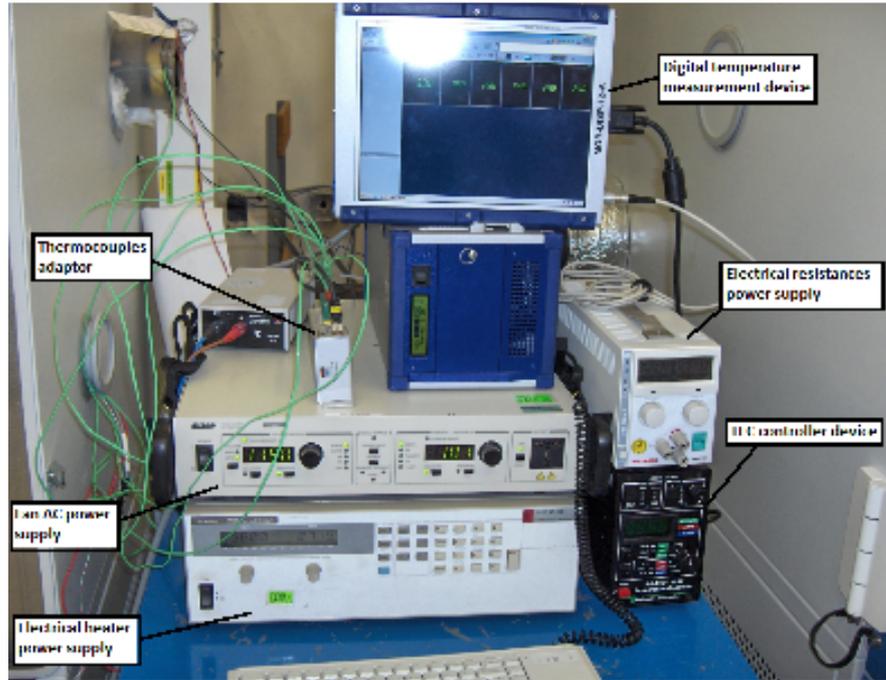
Figure 5.21 The Used Measurement, Controller and Power Devices

Since the forced air will cool the heat sink of the laser pumping chamber, the air velocity values from the POD openings to the heat sink of the laser chamber have been measured by using hot-wire anemometers. In Table 5.1, measured ratings can be observed.

Table 5.1 ExitAir Flow Rate at Different Fan Ratings

	Axial Fan Ratings				
	115 V at 400 Hz	85 V at 400 Hz	75 V at 400 Hz	115 V at 420 Hz	115 V at 380 Hz
Exit Flow Rate (m^3 / min)	2.97	2.29	2	2.8	2.75

5.2 Procedure of the POD Experiments

Firstly the thermal boundary conditions have been provided based on the device operational conditions. The worst case of all parameters have been selected and applied during the experiment. The maximum ambient temperature and the minimum air flow rate conditions have been supplied in the experiments.

The aim of these experiments is to maintain the diode holder at around 50°C in any time whether the heat is generated or not. Before the diodes are started to operate, diode holder temperature should be maintained around 50°C in order to get a high quality laser output with high efficiency.

The experiments have been proceeded in the sequence below;

1. The ambient temperature in the furnace is set to 40°C and waited for a time until the component's temperature reaches this value.
2. Next the air in the plastic duct is supplied at 32°C with small deviations by applying necessary voltage to the fan.
3. As soon as the desired inlet air temperature is obtained, TEC controller device is activated by setting the thermistor resistance so that the diode holders can be maintained at around 50°C.
4. After observing the diode holder temperature is stabilized around 50°C the heat load is applied by the electrical resistances on the diode holders and the TEC controller thermistor resistance is set again.
5. The temperature readings of the thermocouples are observed for a period of time.

While heat generation was not present in the system, the TEC controller drives the TEC module in the negative direction and heat is removed from heat sink to the diode holder region since the target temperature is 50°C in an ambient of 40°C. Since the thermistor is mounted at a location different from diode holders, the set thermistor resistance should be tuned again after applying the heat load.

5.3 The Conducted POD Experiments

In this thesis, TEC cooling of a laser system has been studied. Therefore the temperature distribution has been determined and plotted uniformly against the time. In Figure 5.22, the temperature records of the thermocouples may be seen which are collected after completing Item 3 of the experimental procedure.
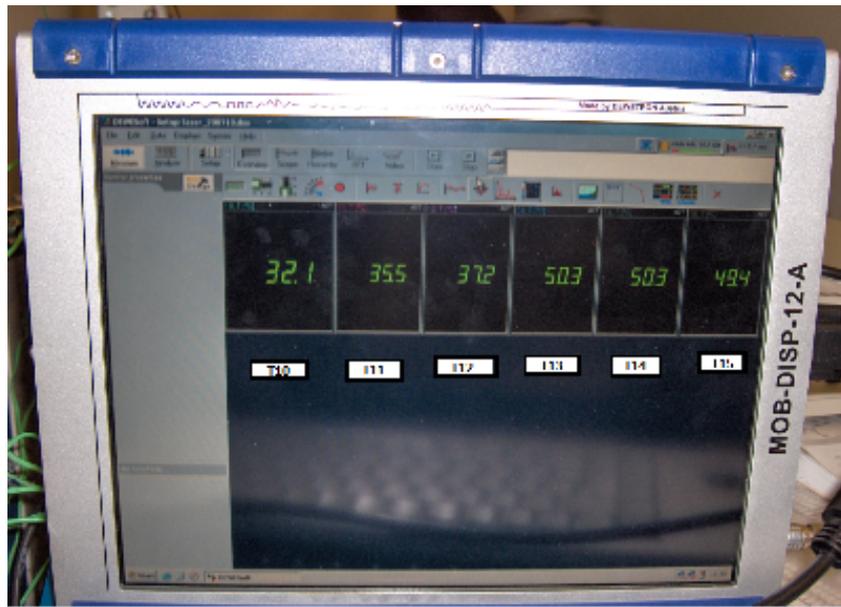
Figure 5.22 Temperature Data before Applying the Heat Load

As it may be observed from the temperature distribution until the diode holders reach the required 50°C, the heat load was not applied. At this stage, TEC module operates in the negative direction with I_{TEC}= -1.2 A and V_{TEC}= -3.5 V ratings. 60 s after the temperature stabilization of diode holders, Item 4 of the experimental procedure has been implemented. The input parameters are shown in the Table 5.2.

Table 5.1 Experiment #1Input Parameters

Experiment #1	Electrically 2 series 2 parallel TECs (2SX2P TEC)					
Input Data	T_{amb} (°C)	P_e (W)	V_{fan} (V)	V_{flow} (m^3/min)	R_{set} (Ω)	T_{set} (°C)
	40	30.1	115 V- 400 Hz	2.97	4.04	47

The experiments lasted around 10 minutes as long as it is possible in order to determine the affecting parameters, although the maximum device operation time will be 6 minutes. Too long working time is not problem for the TEC module as long as its hot side temperature does not exceed the upper limit of 60°C. This longer working time also gives important information on the transient and steady state regimes. In addition, important feedback on the performance of the heat sink and the laser source material performance has been obtained. The temperature data of the thermocouples are listed in Table 5.3;

Table 5.2 Experiment #1 Temperature Records versus Time

Time (s)	T10 (°C)	T11 (°C)	T12 (°C)	T13 (°C)	T14 (°C)	T15 (°C)
0	32.10	35.47	37.16	50.20	50.19	49.39
10	32.54	35.48	37.14	50.20	50.18	49.37
20	32.53	35.49	37.15	50.20	50.17	49.36
30	32.79	35.52	37.18	50.21	50.18	49.36
40	32.96	35.54	37.19	50.20	50.19	49.37
50	32.92	35.58	37.23	50.24	50.22	49.39
60	32.75	35.59	37.24	50.25	50.22	49.40
70	32.74	35.61	37.27	50.21	50.24	49.42
80	32.57	35.65	37.40	48.91	50.06	49.42
90	32.44	35.74	37.62	47.89	49.88	49.57
100	32.38	35.85	37.79	47.44	49.82	49.78
110	32.36	35.96	37.96	47.27	49.87	50.01

Table 5.3 (continued)

120	32.22	36.10	38.14	47.17	49.89	50.19
130	32.15	36.20	38.29	47.03	49.85	50.30
140	32.21	36.33	38.46	46.90	49.78	50.35
150	32.07	36.47	38.63	46.76	49.67	50.40
160	31.86	36.58	38.80	46.59	49.54	50.36
170	31.99	36.72	38.98	46.49	49.41	50.34
180	31.87	36.85	39.14	46.37	49.27	50.27
190	31.91	36.96	39.28	46.25	49.15	50.22
200	31.97	37.07	39.43	46.16	49.04	50.19
210	31.77	37.21	39.58	46.07	48.94	50.14
220	31.77	37.34	39.71	46.01	48.89	50.09
230	31.92	37.45	39.82	45.97	48.82	50.05
240	32.11	37.57	39.92	45.93	48.78	50.01
250	31.85	37.67	40.03	45.90	48.73	49.99
260	31.70	37.75	40.14	45.87	48.71	49.98
270	31.84	37.85	40.23	45.84	48.69	49.98
280	31.90	37.94	40.33	45.85	48.68	49.95
290	31.91	38.03	40.41	45.83	48.66	49.96
300	31.85	38.12	40.49	45.82	48.64	49.95
310	31.88	38.19	40.56	45.81	48.63	49.96
320	32.02	38.28	40.65	45.80	48.62	49.95
330	32.23	38.35	40.70	45.79	48.61	49.97
340	32.29	38.43	40.77	45.78	48.60	49.98
350	32.32	38.50	40.84	45.78	48.57	49.98
360	32.11	38.54	40.93	45.78	48.57	49.97
370	32.09	38.61	40.99	45.77	48.56	49.97
380	31.96	38.68	41.05	45.76	48.55	49.98
390	31.79	38.70	41.08	45.72	48.50	49.94
400	31.80	38.70	41.10	45.66	48.45	49.90
410	31.96	38.75	41.13	45.64	48.42	49.87
420	32.09	38.79	41.18	45.61	48.41	49.86
430	32.37	38.85	41.24	45.61	48.41	49.87
440	32.35	38.91	41.30	45.61	48.41	49.86
450	32.21	38.96	41.35	45.61	48.40	49.86
460	32.30	39.02	41.39	45.62	48.39	49.87
470	32.24	39.08	41.42	45.61	48.40	49.85
480	32.29	39.13	41.47	45.60	48.39	49.85
490	32.26	39.17	41.51	45.59	48.39	49.87
500	32.08	39.20	41.57	45.60	48.40	49.85
510	32.03	39.22	41.60	45.60	48.39	49.83
520	31.91	39.26	41.64	45.60	48.39	49.85
530	31.90	39.29	41.68	45.59	48.38	49.85
540	32.15	39.32	41.71	45.58	48.37	49.84

Table 5.3 (continued)

550	32.06	39.34	41.71	45.54	48.33	49.81
560	32.08	39.32	41.71	45.51	48.30	49.75
570	32.21	39.33	41.73	45.49	48.30	49.73
580	32.19	39.37	41.76	45.49	48.29	49.74
590	31.72	39.40	41.78	45.48	48.30	49.73
600	31.68	39.41	41.81	45.49	48.31	49.73
610	32.05	39.44	41.82	45.49	48.30	49.73
620	32.16	39.47	41.85	45.50	48.30	49.72
630	32.13	39.49	41.90	45.49	48.30	49.72
640	32.15	39.52	41.90	45.50	48.31	49.70

If the temperature records are plotted against to time, the temperature changes of the selected regions may be observed in Figure 5.23;

Figure 5.23 Temperature Variations of the Controlled Regions of Experiment #1

After 10 minutes from the application of the heat load, the TEC module parameters have been listed in Table 5.4;

Table 5.3 Output Parameters of the TEC Module in Experiment #1

Output Data	$R_{measured}$ (Ω)	$T_{measured}$ ($^\circ$C)	I_{TEC} (A)	V_{TEC} (V)	P_{TEC} (W)
t: 600s	4.04	47	0.77	1.33	1.02

If the output temperatures of the Experiment #1 are evaluated, it may be said that a good cooling performance is obtained with the fast response of the TEC modules. In the temperature variation graph, it is seen that the cooling started at the 60th second which is the time of applying the heat load from the diode holders. At this time, TEC controller starts to operate in the positive direction and pulls down the temperature of the base plate (T13) in order to remove the heat load from the diode holders and maintain them at around 50°C (T14 and T15). This transition range takes place for about 140 s and in this period the diode holder temperatures have an increase but do not exceeding the safe operational limits. If the TEC controller thermistor is placed on one of the diode holders, lower temperature variation at T14 and T15 will be observed in the transition range.

At 200 s, the temperatures begin to saturate and the diode holder temperatures (T14 and T15) decrease since the base plate temperature (T13) is pulled down to the required level. The difference between the two diode holder temperatures comes from the copper to copper surface contact quality of the components. This means that the parts should be machined more precisely. The two holders may have different surface tolerances as a result different contact resistance values occurred. Besides that, a hotter diode holder can mean the lower performance of the TEC module. In theory, if all the assembling tips and rules are obeyed, the four TEC modules must show the same performance. However, if the base plate is twisted during the integration or the thickness of the thermal interface material differs for each TEC, the TEC modules show different characteristics.

During both the transition and the saturation periods, the heat sink temperatures at the near and far regions of the hot spot (T11 and T12) always increase which is the result of uniform heat removal from the base to the heat sink with the positive operational direction of the TEC module. It can be seen that pumped air temperature (T10) from the plastic duct fluctuates in the very small range and stays around the 32°C. TEC module current and voltage ratings show that the module operates in the very safe region with very low input power. The total heat removed from the heat sink can be calculated as 30+1.02 = 31.02 W. As a result desired cooling performance is obtained when 30 W heat load is applied in Experiment #1 and the system can operate at least 10 minutes in this condition.

Experiment #2 has been conducted by only changing the heat load from the previous one (Experiment #1) with input values shown in Table 5.5.

Table 5.4 Experiment #2 Input Parameters

Experiment #2	Electrically 2 series 2 parallel TECs (2SX2P TEC)				
Input Data	T_{amb} (°C)	P_e (W)	V_{fan} (V)	V_{flow} m^3 / min	R_{set} (Ω)	T_{set} (°C)
	40	40	115 V- 400 Hz	2.97	4.36	45

As it may be observed from the Table 5.5, when the applied heat load is increased, the TEC controller set temperature in the base plate is decreased. This temperature reduction is required for maintaining the diode holder temperatures at the desired level when exposed to higher heat load.

Temperature data collected from the thermocouples are listed in the Table 5.6;

86

Table 5.5 Experiment #2 Temperature Records versus Time

Time (s)	T10 (°C)	T11 (°C)	T12 (°C)	T13 (°C)	T14 (°C)	T15 (°C)
0	32.43	35.95	37.66	50.18	50.21	49.17
10	32.37	35.93	37.63	50.17	50.21	49.17
20	32.41	35.89	37.60	50.15	50.19	49.13
30	32.29	35.85	37.59	50.16	50.20	49.13
40	32.17	35.81	37.53	50.15	50.19	49.13
50	32.14	35.80	37.52	50.14	50.20	49.11
60	32.35	35.79	37.55	49.41	50.01	48.97
70	32.34	35.82	37.72	47.96	49.54	48.91
80	32.54	35.90	37.87	47.31	49.74	49.49
90	32.58	36.01	38.02	47.10	50.10	50.16
100	32.53	36.13	38.21	47.04	50.39	50.74
110	32.38	36.27	38.43	46.98	50.55	51.20
120	32.27	36.41	38.65	46.87	50.59	51.55
130	32.20	36.59	38.94	46.72	50.53	51.74
140	32.23	36.75	39.23	46.55	50.39	51.82
150	32.10	36.94	39.50	46.37	50.24	51.83
160	32.21	37.13	39.80	46.20	50.09	51.80
170	32.33	37.34	40.05	46.03	49.93	51.71
180	32.41	37.54	40.31	45.89	49.79	51.61
190	32.25	37.74	40.54	45.78	49.66	51.48
200	32.11	37.92	40.76	45.69	49.53	51.40
210	32.08	38.12	40.98	45.59	49.47	51.30
220	32.20	38.32	41.17	45.51	49.38	51.22
230	32.26	38.48	41.35	45.47	49.31	51.15
240	32.29	38.64	41.51	45.41	49.27	51.10
250	32.38	38.83	41.66	45.36	49.21	51.04
260	32.37	38.97	41.82	45.33	49.18	51.01
270	32.43	39.13	41.98	45.31	49.15	50.99
280	32.40	39.26	42.10	45.30	49.12	50.95
290	32.57	39.40	42.25	45.26	49.12	50.93
300	32.59	39.55	42.39	45.26	49.09	50.93
310	32.65	39.67	42.52	45.22	49.09	50.91
320	32.68	39.81	42.63	45.21	49.06	50.91
330	32.68	39.93	42.75	45.19	49.05	50.89
340	32.76	40.04	42.87	45.17	49.02	50.87
350	32.72	40.15	42.97	45.15	49.00	50.86
360	32.83	40.27	43.08	45.11	48.99	50.84
370	32.63	40.38	43.18	45.11	48.97	50.83
380	32.55	40.48	43.30	45.10	48.96	50.80
390	32.67	40.57	43.41	45.09	48.93	50.79
400	32.65	40.66	43.51	45.06	48.89	50.76
410	32.63	40.73	43.57	45.01	48.87	50.72

Table 5.6 (continued)

420	32.69	40.80	43.66	44.98	48.84	50.69
430	32.72	40.88	43.74	44.96	48.80	50.66
440	32.79	40.97	43.83	44.93	48.80	50.65
450	32.58	41.03	43.88	44.89	48.75	50.61
460	32.49	41.11	43.97	44.88	48.74	50.60
470	32.45	41.19	44.06	44.87	48.73	50.58
480	32.35	41.24	44.13	44.83	48.70	50.55
490	32.40	41.32	44.22	44.81	48.70	50.53
500	32.29	41.38	44.29	44.81	48.69	50.51
510	32.32	41.43	44.32	44.80	48.69	50.49
520	32.42	41.50	44.40	44.78	48.68	50.48
530	32.49	41.55	44.46	44.76	48.68	50.45
540	32.54	41.61	44.52	44.75	48.66	50.44
550	32.52	41.68	44.59	44.73	48.64	50.43
560	32.60	41.75	44.64	44.72	48.64	50.42
570	32.44	41.82	44.71	44.72	48.65	50.40
580	32.40	41.85	44.76	44.71	48.62	50.39
590	32.29	41.90	44.81	44.69	48.61	50.38
600	32.09	41.96	44.88	44.68	48.61	50.39
610	32.14	42.00	44.91	44.67	48.59	50.37
620	32.22	42.04	44.97	44.67	48.58	50.37
630	32.20	42.08	45.02	44.65	48.58	50.35

The plotted temperature records against the time can be found in Figure 5.24.
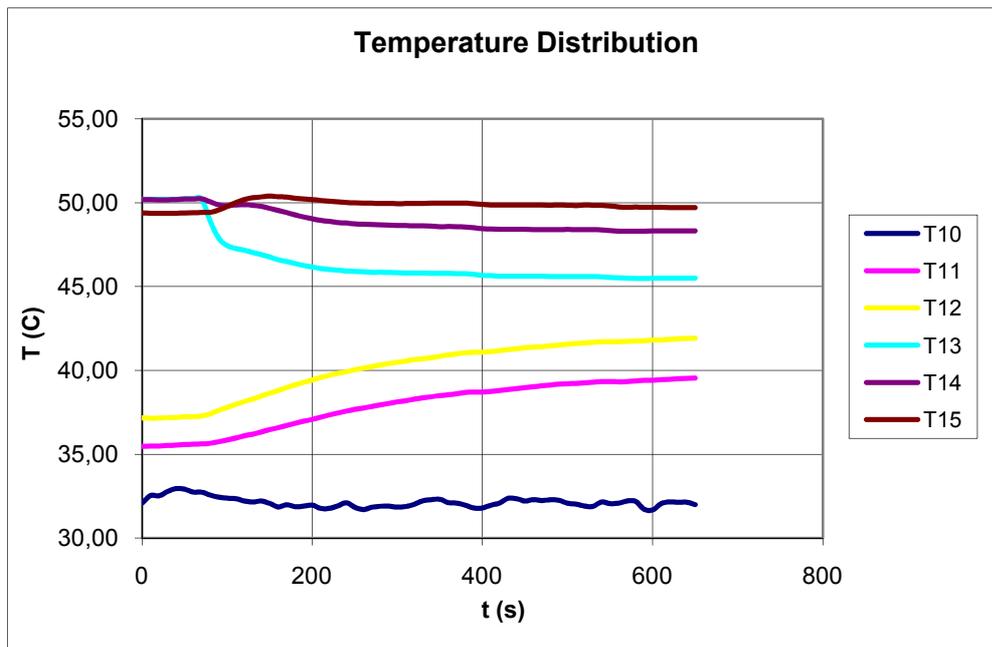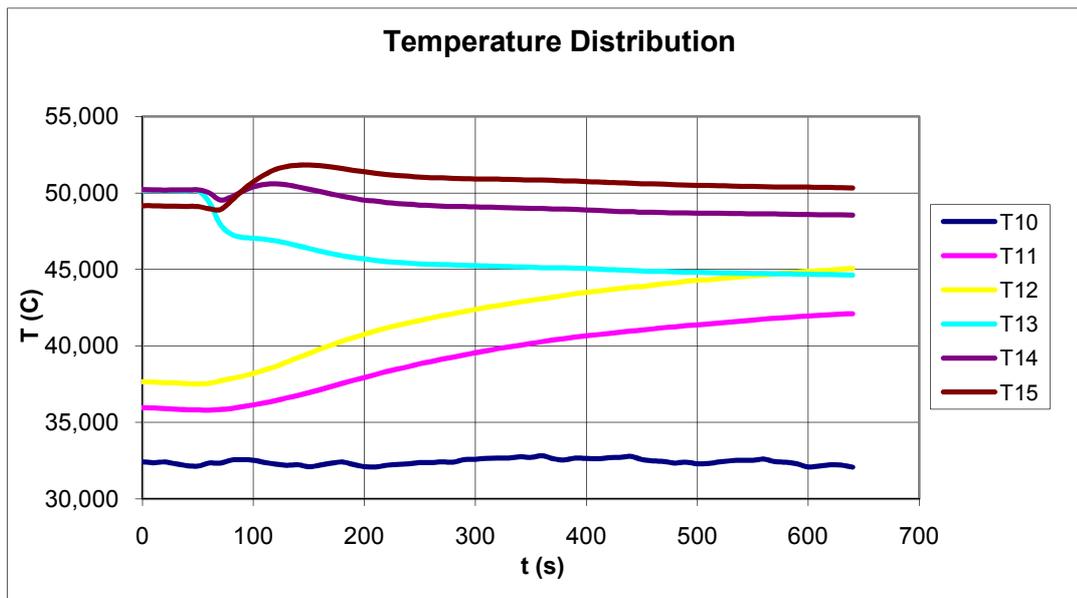

Figure 5.24 Temperature Variations of the Controlled Regions of Experiment #2

10 minutes after the application of the heat load, the resulting parameters can be found in Table 5.7;

Table 5.6 Output Parameters of the TEC Module in Experiment #2

Output Data	$R_{measured}$ (Ω)	$T_{measured}$ (°C)	I_{TEC} (A)	V_{TEC} (V)	P_{TEC} (W)
t: 600s	4.36	45	1.89	3.78	7.2

In Experiment #2, it may be seen that the cooling started again at the 60th second which is the time of applying the heat load. After that time, the same transition period takes place for about 140-150 s and in this period the diode holder temperatures have greater increase but not exceeding the safe operational limits. The duration of the transition period did not differ very much because of the TEC controller sensitivity. The controller drives the TEC module with more input power and higher cooling capacity in the case of higher applied heat load.

In the transition region, it is apparent that temperature readings on the same thermocouple are greater compared to those in the 1st experiment because of the higher heat load. Moreover, it may be seen more clearly that the surface thermal resistance of diode holder1 is greater than that of diode holder 2. This difference can be detected from both heating and cooling regime diode holder temperatures (T14 and T15). As in Experiment #1, when time shows 200 s, temperature values start to saturate and the diode holder temperatures (T14 and T15) decrease since the base plate temperature (T13) is pulled down to the required level.

The heat sink temperatures T11 and T12 are again in the increasing trend but more rapidly because of the higher heat load. In order to remove the higher heat load from the heat sink, a higher temperature gradient between the heat sink and the ambient is required. The pumped air temperature T10 seems uniform around 32°C again. It has been observed that the TEC module operates with a higher input power 7.2 W but

still in the safe region. The total heat removed from the heat sink can be calculated as 40+7.2 = 47.2 W. At the end of experiment#2, the desired cooling performance is obtained when 40 W heat load is applied and the system can operate at least 10 minutes with higher heat sink temperatures.

Experiment #3 is implemented with the same conditions as the CFD (Fluent) analysis performed in Chapter 4. The input parameters can be found in the Table 5.8.

Table 5.7 Experiment #3 Input Parameters

Experiment #3	Electrically 2 series 2 parallel TECs (2SX2P TEC)					
Input	T_{amb}	P_e	V_{fan}	V_{flow}	R_{set}	T_{set}
Data	(°C)	(W)	(V)	(m^3 / min)	(Ω)	(°C)
	40	46	85 V-400 Hz	2.29	4.44	44.5

Results are presented in the Table 5.9 and Figure 5.25;

Table 5.8 Experiment #3 Temperature Records versus Time

Time (s)	T10 (°C)	T11 (°C)	T12 (°C)	T13 (°C)	T14 (°C)	T15 (°C)
0	31.53	37.85	39.31	49.71	49.67	49.12
10	31.23	37.75	39.22	49.71	49.69	49.14
20	31.38	37.67	39.15	49.72	49.69	49.14
30	31.32	37.60	39.07	49.73	49.70	49.16
40	31.05	37.51	38.98	49.75	49.71	49.17
50	31.09	37.42	38.91	49.46	49.67	49.14
60	31.41	37.39	39.06	47.77	48.98	48.69
70	31.38	37.42	39.25	46.56	48.76	48.88
80	31.06	37.49	39.39	46.22	49.19	49.62
90	30.79	37.56	39.54	46.23	49.70	50.39
100	30.70	37.64	39.72	46.32	50.14	51.02
110	30.64	37.74	39.97	46.36	50.41	51.49
120	30.52	37.88	40.26	46.34	50.57	51.80
130	30.52	38.04	40.60	46.26	50.62	51.98

90

Table 5.9 (continued)

140	30.71	38.22	40.92	46.12	50.60	52.09
150	30.91	38.43	41.28	45.97	50.48	52.09
160	30.95	38.61	41.59	45.81	50.36	52.04
170	30.97	38.85	41.89	45.66	50.22	51.98
180	31.17	39.08	42.18	45.52	50.09	51.88
190	31.13	39.31	42.49	45.39	49.96	51.78
200	31.22	39.54	42.77	45.27	49.84	51.70
210	31.11	39.77	43.01	45.18	49.72	51.62
220	31.14	39.99	43.25	45.11	49.64	51.54
230	31.16	40.23	43.50	45.06	49.57	51.47
240	31.28	40.44	43.71	45.00	49.50	51.40
250	31.28	40.63	43.93	44.94	49.46	51.33
260	31.10	40.81	44.11	44.87	49.38	51.27
270	30.99	40.96	44.27	44.81	49.31	51.20
280	31.08	41.14	44.44	44.78	49.28	51.15
290	31.25	41.32	44.65	44.75	49.26	51.12
300	31.29	41.50	44.86	44.74	49.22	51.11
310	31.26	41.68	45.03	44.72	49.22	51.10
320	31.39	41.87	45.21	44.70	49.21	51.10
330	31.63	42.04	45.38	44.69	49.20	51.08
340	31.75	42.19	45.56	44.68	49.20	51.07
350	31.87	42.37	45.73	44.66	49.20	51.06
360	32.14	42.50	45.85	44.63	49.14	51.03
370	32.15	42.62	45.96	44.56	49.08	50.96
380	32.35	42.78	46.13	44.55	49.07	50.95
390	32.34	42.92	46.30	44.53	49.06	50.93
400	32.23	43.07	46.46	44.52	49.04	50.92
410	32.27	43.24	46.60	44.51	49.04	50.91
420	32.52	43.40	46.78	44.50	49.03	50.90
430	32.58	43.55	46.92	44.48	49.02	50.90
440	32.41	43.68	47.08	44.47	49.01	50.89
450	32.43	43.83	47.24	44.45	49.00	50.87
460	32.57	43.93	47.33	44.41	48.96	50.84
470	32.68	44.04	47.43	44.34	48.91	50.77
480	32.57	44.17	47.57	44.31	48.85	50.73
490	32.79	44.30	47.71	44.30	48.85	50.71
500	32.84	44.44	47.85	44.30	48.84	50.69
510	32.84	44.57	48.00	44.29	48.84	50.68
520	32.67	44.71	48.13	44.28	48.81	50.67
530	32.66	44.83	48.26	44.26	48.79	50.64
540	32.56	44.97	48.40	44.25	48.80	50.63
550	32.41	45.09	48.54	44.23	48.78	50.61
560	32.43	45.20	48.64	44.21	48.77	50.60
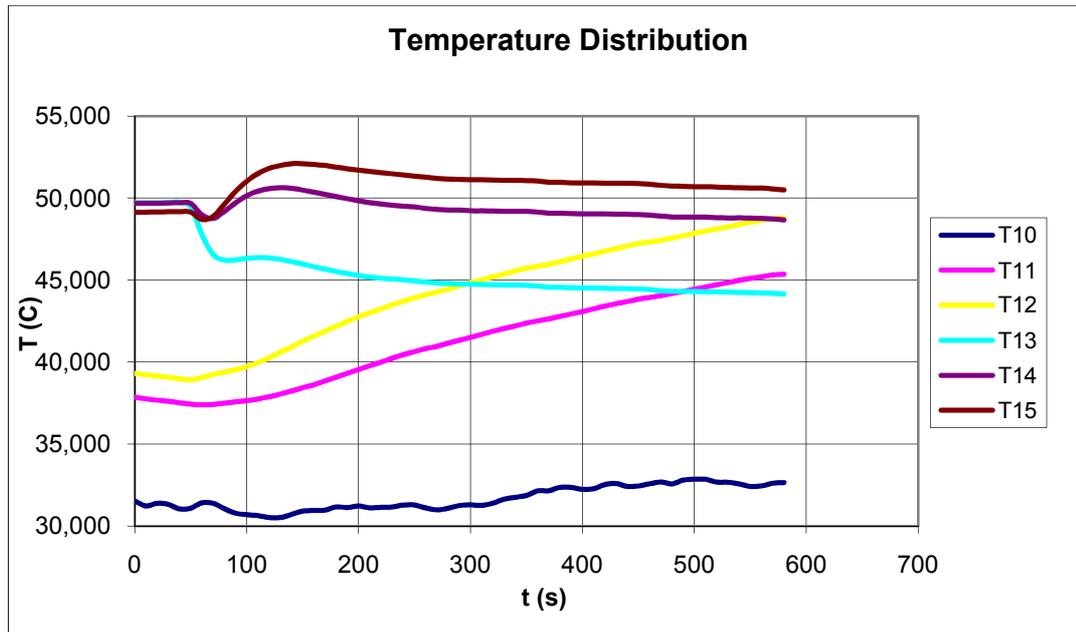
Figure 5.25 Temperature Variations of the Controlled Regions of Experiment #3

The resulting parameters of Experiment #3 may be found in Table 5.10.

Table 5.9 Output Values of TEC Module in Experiment #3

Output Data	$R_{measured}$ (Ω)	$T_{measured}$ (°C)	I_{TEC} (A)	V_{TEC} (V)	P_{TEC} (W)
t: 200 s	4.25	45.2	1.8	3.95	7.1
t: 300 s	4.44	44.5	2.35	4.7	11.1
t: 360 s	4.44	44.5	2.65	5.41	14.3
t: 580 s	4.44	44.5	2.97	6.1	18.1

In this experiment, since the total heat load is tried to be maintained the same as that in the CFD (Fluent) analysis, different TEC current and voltage ratings have been recorded at corresponding times.

In Experiment #3, the diode holder temperatures T14 and T15 have been maintained in the safe temperature limits, although higher heat load is applied with smaller flow rate. As it is seen in the Figure 5.25, similar transition and saturation profiles are obtained as in the previous experiments. The transition period does not show big differences among the three cases because of the closed loop control of the TEC module. The performance of the TEC controller can be observed from the base plate temperature T13 which is very close to the set temperature 44.5°C in the saturation regime. Temperature variations in the same thermocouple measurements are slightly higher than those in Experiment #2 because of the higher heat load, and lower flow rate.

The heat sink temperatures T11 and T12 are so much higher than those in Experiment #2. From the two graphs it may be seen that T12 reaches 45°C at 300 s in this experiment. However in Experiment #2, this duration is 600 s. This important difference comes mainly from the higher heat load, lower flow rate and the higher TEC input power. It is known that the TEC module operates with a higher input power as the heat load is increased. Moreover, if the thermal resistance of the heat sink is increased by lowering the forced air flow rate, the TEC module tries to increase the hot side temperature (T_h) and again operates with higher input powers. The pumped air flow rate temperature T10 is kept uniform around 32°C during the experiment.

The input power of TEC increases as the cooling period gets closer to the steady state regime. This means that the heat load is firstly accumulated in the copper heat sink and then removed to ambient by convective cooling. Until the copper heat sink is completely filled, the transient regime is dominant and the heat sink thermal resistance is lower when compared to steady state heat sink thermal resistance.

5.4   Comparison of the Results of the CFD Analysis and Experiment #3

In the CFD analysis air flow rate of 2.3 m^3/min at 32°C was defined and a copper heat sink structure within the same geometry and control volume has been tested. The ambient temperature was also taken as 40°C. These conditions were the same as those in Experiment #3. As mentioned before total applied heat load is equal to 60 W from the four TEC modules.

If the results of the CFD modeling and the experiments are compared, the system may be said to operate safely for both cases. However, the temperature variation and the maximum temperature values show differences among each other. Since the device maximum operational time is limited to 6 minutes, this duration has been taken as reference for the comparison.

In the Experiment #3, the heat sink temperatures vary about 6°C after applying the heat load at the 60th second until 420th second. In the analysis, the temperature variation is about 11°C until the 360th second.

The average heat sink temperature of the CFD analysis at 360th second was 53°C as can be read from the Figure 4.12. Moreover, the heat sink temperatures T11 and T12 are 43.4°C and 46.8°C respectively when the time is 420 second from the Figure 5.25. In Experiment #3, the time 420 s is selected instead of 360 s as in the analysis, since the heat load is applied on the system at 60th second.

If the average heat sink temperature is taken as approximated as T12 in Experiment #3 which is 47°C, it is 6°C colder than the CFD analysis result of 53°C. 6°C is important difference between two cases. The possible reasons to this 6°C difference may be stated as follows;

- In the CFD analysis, radiation heat transfer is neglected. However, in the Experiment #3, radiation exists due to the considerable temperature difference between laser source and housing components.

- In the CFD analysis, the 60 W heat load was directly applied on the heat sink from the beginning of the analysis. In the experiment, although the applied heat load from electrical resistances does not change, the TEC input power increases with time. Hence, the total heat load varies with time.

- In the analysis the average heat sink initial temperature was 42°C though in the experiment, it was around 39°C (T12).

- Since the whole system is composed of many mechanical components and the system is very sensitive to the thermal boundary conditions, the two structures may have small geometrical differences in volume and area base.

- The mesh structure of the analysis may be improved with a higher quality mesh.

- Experimental uncertainty may also play an important role.

As a final experiment (Experiment #4), the heat load was increased to 50 W and keeping all other input parameters the same, the measurements have been repeated. Safe operation of the POD system has been observed. The results may be seen in Appendix A.

CHAPTER 6

DISCUSSIONS AND CONCLUSIONS

6.1   Summary and Conclusions

In this thesis, experimental application of the recent technology TEC devices has been performed for cooling diode pumped laser system. The experiments and the proceeding design stages have been supported by a CFD model of the laser system in order to decide on the mechanical and thermal design alternatives. The main heat generators are the laser diodes in the system and heat load calculations have been carried out based on the maximum heat generation mode which is the 20 Hz operating condition. The most convenient mechanical configuration of the laser source and the TEC module has been decided depending upon the heat load distribution and the thermal requirements of the laser source components. Later, preliminary design experiments have been performed with TEC coupled pumping chamber with heat sink in order to examine TEC mounting and to specify other system parameters.

In order to simulate the heat sink and achieve the most efficient TEC integration, the assembly tips of the TEC module has been implemented using available thermal materials and cooling components. TEC devices are very sensitive to mechanical, thermal shock and loads; hence the manipulation of TEC devices needs great care. The performance of the TEC module has been checked by an AC resistance measurement.

After constructing the TEC assembly, the total heat generation on the system has been simulated by the electrical resistances mounted on diode holders. 20 Hz working condition corresponds to the maximum reputation rate and maximum heat generation mode has been taken as reference while applying heat load on resistances. The laser source and heat sink system was then equipped with thermocouples and sealed within a rapid prototype plastic housing. The completed system was then placed in the furnace and the TEC closed loop controller device and the DC current fan connections were made. Several experimental data have been collected by tuning the temperature of the furnace, amount of the heat load and the air flow rate. From the controlled experiments, the TEC module behavior has been found reasonable in response to changing parameters. The thermocouples used to measure the instant temperatures from the critical regions provide very important information. By using the temperature data, the hot and the cold surface temperatures of TEC device, contact thermal resistance between the TEC device and the heat sink and the base plate can be calculated.

The TEC controller simplifies the TEC module operation very much which can be set to the required temperatures by entering its thermistor resistance value. The efficiency and the C.O.P of the TEC module may also be calculated by taking the input current and the voltage values from the TEC controller device. The air flow rate determined from the free flow performance curve of the DC fan using the input power of the fan. The temperature data from different points on the heat sink provided important feedback on the geometrical design of the heat sink of POD system. TEC module embedded IcePak simulation of the heat sink-fan system was driven with the same boundary conditions. The heat load distribution and temperature data obtained from the two studies have been compared for various surface contact impedance values between the components. The temperature data are seemed similar to each other at the thermal impedance values that should be improved by using high quality thermal pads.

After gaining experience from first experiments, the base plate, diode holders geometries and thermal interface materials have been selected and the outer heat sink material and the fin geometry have been tried to be optimized by making a series of IcePak simulations. Using the Fluent CFD program, different types of fin geometries of heat sink models are formed and performances are simulated. The laser device has cooling air supply that provides impinging flow on to the heat sink. Firstly, the individual device components and an independent control volume configuration have been formed with parallel plain fins. It has been seen that air flow orientation was not in the desired level with this type of fins. Heat is localized on the hot spot and the air flow is going through insufficient amount of fin passages. In order to decrease the heat localization, a copper heat sink with a thicker base plate was considered and an improvement has been obtained in the temperature distribution and the maximum temperature values. According to the simulation results, it seems that planar plain fin geometry was found more efficient than pin fin geometry. Also, an improvement in the fin geometry was found to orient flow through the hot spot region.

By considering the experimental observations and the simulation results; a new curved shaped planar finned heat sink model has been constructed in order to meet the cooling and air flow requirements. An additional air orienting duct has been integrated with the heat sink to improve the air flow area. The complete POD assembly was formed by constructing the main components besides the air entering openings and the duct components. First, a transient analysis with an aluminum heat sink has been completed using the worst boundary conditions. The velocity profile around the fins and the hot spot was improved. The orienting duct has great effect on this improvement. It has been seen that the hot spot was localized on aluminum heat sink and reached a maximum of 67°C. It has been observed that the area of the hot spot on the aluminum heat sink should be enlarged and the average temperature should be decreased.

Next, a copper heat sink model was analyzed within the same boundary conditions. Better temperature profiles have been obtained with the copper heat sink. On the

other hand, the same velocity profile was obtained because of the same geometry and the pumping rate. The maximum temperature was obtained in the hot spot as 59°C which is 8°C lower than that in the aluminum heat sink.

After observing the thermal performance of the system with the CFD analysis, experiments have been conducted on the POD system which consists of different type devices such as infrared camera, receiver optical assembly and laser designating device etc. Except the laser pumping chamber with heat sink, an SLA prototype model of the sensors and electrical boards have been manufactured.

The laser designating device (TEC coupled laser pumping chamber, heat sink) is constructed in the sequence of the assembly components by obeying TEC assembling tips. A copper heat sink is used with a graphite based thermal pad which has good thermal properties and flexible characteristics. Because of the very small thickness of the pad and the high conductivity yielded very low thermal impedance values. Moreover, the flexibility of the pad could compensate the surface tolerance deviations and supply good surface contact which also results in low thermal impedance values. Electrical resistances have been used to simulate the heat generation.

Since the environmental control unit (ECU) was still under construction, an alternative cooling system was designed for the experiments. A plastic component was manufactured with the rapid prototype technique which has a duct function when connected to the channel of the wing part of the POD system. The air duct assembly was connected to the outer POD housing and put in the furnace.

A series of experiments on the POD system have been performed by changing the heat load and the air flow rate. The temperature distribution has been plotted with respect to time. It can be said that good cooling performance has been obtained with the fast response of TEC modules in most of the experiments. Since the TEC controller thermistor was away from the diode holders, a transition range has been

observed at the beginning of the cooling regime but the temperature of the diode holders do not exceed the allowable working limits.

If the experimental results are compared with the CFD results, the temperature variation and the maximum temperature values of the heat sink show some differences. An important average temperature difference of 6°C has been observed between the experimental data and the CFD results. This difference may come from not taking the radiation heat transfer into account, from the amount of accumulated heat load and from the difference in initial temperatures of heat sink in experiment and in CFD simulation.

In conclusion, a thermoelectrically cooled laser designating device with copper heat sink of curved planar fins has been designed, simulated, manufactured and tested. The device has been shown to operate longer than the required operational time under worst boundary conditions. The safe operation of the TECs within their recommended region of the performance curve has been ensured with a high C.O.P value.

6.2   Recommendations

During the design stages, the operational conditions of the laser device usually have variations and should be frequently revised due to the crowded inner control volume of the pod system. Since the whole POD system consists of many equipments, namely, the electronics, infrared and laser devices, the working boundary conditions of each device should be observed with care. The air flow rate supplied to the heat sink of the laser device, the ambient temperature and the pumped air temperature values may vary during the operation. The allocated space for the laser device in the targeting pod system may be made larger which simplifies the mechanical configuration of the components and enables larger heat transfer area.

More efficient laser diodes may be used which have higher light conversion percent that means less cooling requirement. Also, more endurable diodes may be selected which can work at higher temperatures and need less amount of cooling.

The integration of the TEC module may be performed with more suitable interface materials and cooling components so that possible damages to the TEC can be reduced.

Instead of dealing with four different TEC devices, one customly designed product may be used though it can be more expensive. One bigger TEC device with the same cross section area of the present four TEC may greatly simplify the assembly and the power requirements.

During the experiments, temperature data have been collected from the target points by thermocouples with insert type tips which take local data. Also, a stiffener was required to mount thermocouple firmly. Thermocouples which allow more uniform temperature measurement can be used and easily mounted thermocouples may be selected.

A combined power supply, measurement and controller unit may be used instead of separate units. This simplifies the experimental procedure and shortens the duration of the experiments.

In the POD experiments, devices other than the laser designator have been manufactured using a plastic material by rapid prototyping. The effects of the heat generated in the complete pod inner volume composed of actual devices on the laser cooling may be examined as a future work.

The heat generation on the laser device was simulated by electrical resistances on diode holders. If the diode pumps are not very expensive units, they can be directly driven for heat generation in the experiment. Experiments on the completed laser

device will yield more reasonable results possibly agreeing better with the simulations.

During the construction of the laser source, copper diode holders have been placed with copper to copper surface contact which causes high thermal resistance between the components. As long as the elevation of the diodes with respect to the laser crystal is not affected much, a high conductive thin thermal pad can be used to reduce the thermal contact resistance. This way, the temperature gradient between components can be decreased.

POD experiments showed that the laser device can be cooled with copper laser source components and a copper heat sink. However, copper is a very heavy material that increases the weight of the system very much. The experiments may be repeated with aluminum laser source components and an aluminum heat sink. With aluminum heat sink the laser device is not expected to operate as long as the case with copper heat sink. However, the required operational time may still be achieved with aluminum components.

REFERENCES

[1] http://www.scribd.com/doc/10019268/Laser-Theory, Last visited in July 2010.

[2] John Suarez, ''Introduction to Laser Theory'', Princeton REU Program, Summer 2003.

[3] Antar, Mohammed A., ''Thermal radiation role in conjugate heat transfer across a multiple-cavity blocks'', Environment Complete, Vol. 35, Iss. 8, p. 3508-3516, 2010.

[4] Mahanta, Nayandeep K., Abramson, Alexis R., ''The dual-mode heat flow meter technique: A versatile method for characterizing thermal conductivity'', Academic Search Complete, Vol. 53, p. 5581-5586, 2010.

[5] Tsunekane M., Taira T., ''Design and Performance of Compact Heatsink for High Power Diode Edge-Pumped Microchip Lasers'', IEEE Electronic Library Online, Vol. 13, p. 625, 2007.

[6] Conner M., ''Heat spreaders and fans diffuse hot spots'', Scopus, Vol. 50, p. 55, 2005.

[7] Huang B., Kung K., ''Mode localization of a component water heat exchanger'', International Journal of Mechanical sciences, Vol. 56, p. 170, 2005.

[8] H.B. Lloyd, ''Corrosion Problems in a Blast Furnace Water-Cooling System'', Emerald Journals, Vol. 4, Iss. 7, 1957.

[9] Srinivasan R., Miller R., Kuppuswamy K., ''Next generation active and passive heat sink design for diode lasers'', SPIE, The International Society for Optical Engineering, Vol. 6456, p. 205-215, 2007.

[10] M. Fatih Demirbas, ''Thermal Energy Storage and Phase Change Materials: An Overview'', InformaWorld, Vol. 1, Iss. 1, p. 85-95, 2006.

[11] B. V. Kosoy, "Heat Pipes, Theory and Practice", International Centre for Heat and Mass Transfer and Egik Inc. PTC-03 Short Course on Passive Thermal Control, pp. 33-54, October 2003.

[12] G. P. Peterson, "An Introduction to Heat Pipes", John Wiley & Sons, 1994.

[13] ''Thermoelectrics'', The Columbia Encyclopedia, http://www.bartleby.com/65/th/thermoel.html, Last visited in June 2010.

[14] Josh Kimmel, ''Thermoelectric Materials'', Physics 152, Special Topics Paper, 1999.

[15] L.M. Goncalves, C.Couto, P.Alpuim, D.M.Rowe, ''Thermoelectric Properties of Bi_2Te_3 / Sb_2Te_3 Thin Films'', Materials Science Forum, Vols. 514-516, pp. 156-160, 2006.

[16] Michael Freunek, Leonhard M. Reindl, William D., ''Modified Model for Thermoelectric Generators'', Technology Report of the Laboratory of Electrical Instrumentation, Department of Microsystems Engineering (IMTEK), 2007.

[17] Artur Mirocha, Piotr Dziurdzia, ''Improved Electrothermal Model of the Thermoelectric Generator Implemented in SPICE'', ICSES International Conference On Signals and Electronic Systems, 2008.

[18] Yaakov Kraftmakher, ''Simple Experiments with a Thermoelectric Module'', Eur. J. Phys., Vol.26, p 959–967, 2005.

[19] G. Jeffrey Snyder and Tristan S. Ursell, ''Thermoelectric Efficiency and Compatibility'', Physical Review Letters, Volume 91, Number 14, 2003.

[20] ''Thermoelectric Applications'', Melcor, Thermoelectric Handbook, http://www.melcor.com/handbook.htm, Last visited in August 2010.

[21] David D. Nelson, Barry McManusa, Shawn Urbanski, Scott Herndon, ''High precision measurements of atmospheric nitrous oxide and methane using thermoelectrically cooled mid-infrared quantum cascade lasers and detectors'', ScienceDirect, Spectrochimica Acta Part A 60, 2004.

[22] Marko Labudovic, Jin Li, ''Modeling of TE Cooling of Pump Lasers'', IEEE Transactions on Components and Packaging Technologies, Vol. 20, pp. 230-237, 2007.

[23] Ronggui Yang, Gang Chen, A. Ravi Kumar, G. Jeffrey Snyder, Jean-Pierre Fleurial, ''Transient cooling of thermoelectric coolers and its applications for microdevices'', ScienceDirect, Energy Conversion and Management, Vol. 46, pp. 1407-1421, 2004.

[24] Hee Jin Lee, Joon Shik Yoon, and Charn-Jung Kim, ''Numerical Analysis on the Cooling of a Laser Diode Package with a Thermoelectric Cooler'', Heat Transfer-Asian Research, Vol. 30, pp. 5-10, 2001.

[25] Ioan Sauciuc, Hakan Erturk, Gregory Chrysler, Vikram Bala, Ravi Mahajan, ''Thermal Devices Integrated with Thermoelectric Modules with Applications to CPU Cooling'', Intel Technology Symposium, San Francisco, 2005.

[26] ''Structure and Function'', Melcor, Thermoelectric Engineering Handbook, http://www.melcor.com/handbook.htm, Last visited in August 2010.

[27] Alasdair McInnes and James Richards, ''Thermal Effects in a Coplanar-Pumped Folded-Zigzag Slab Laser'', IEEE Journal of Quantum Electronics, Vol. 32, No. 7, 1996.

[28] http://www.scd.co.il/dynamicweb.aspxpage_id=28&parent_id=0&pgnm=Dio de Lasers, Last visited in August 2010.

[29] Paul R. Stysley, Demetrios Pouliosa, Donald B. Coyleb, Richard B. Kaya, ''Highly efficient dual head 100 mJ TEM Nd:YAG Oscillator'', ScienceDirect , Optics & Laser Technology, Vol. 40, pp. 435-440, 2008.

[30] http://www.icepak.com/index.htm, Last visited in August 2010.

[31] VLOC Inc., http://www.vloc.com//PDFs/YAGBrochure.pdf, Last visited in August 2010.

[32] SCD SemiConductor Devices, https://www.scd.co.il/dynamicweb.aspxpage_id=28&parent_id=0&pgnm=Di ode Lasers, Last visited in August 2010.

[33] Marlow INC., www.marlow.com, Last visited in August 2010.

[34] ''TEC Assemblying Tips and Rules'', Melcor, Thermoelectric Engineering Handbook, http://www.melcor.com/handbook.htm, Last visited in August 2010.

[35] http://www.schreier-metall.de/gclid=CN_rifvtw6MCFUIsDgod5jT, Last visited in August 2010.

[36] GrapTECH Inc., http://www.graftechaet.com/GRAFOIL/GRAFOIL-Products/Single-Layer-Material, Last visited in August 2010.

[37] Yoshihiro Kondo, Hitoshi Matsushima, and Shigeo Ohashi, ''Optimization of Heat Sink Geometries for Impingement Air-Cooling of LSI Packages'', Heat Transfer-Asian Research, Vol. 28, pp. 135-139, 1999.

[38] Melcor, Thermoelectric Engineering Handbook, http://www.melcor.com/handbook.htm, Last visited in August 2010.

[39] Amatek Rotron INC. http://www.ametekaerodefense.com/products/sku.cfmProductCAtegory_Id=4258&Product_Id=1075&SKU_Id=1269, Last visited in August 2010.

[40] Malcom INC., http://www.malcom.com/products/process_heat_tools.php, Last visited in August 2010.

APPENDIX A

POD EXPERIMENT COMPONENTS AND RESULTS
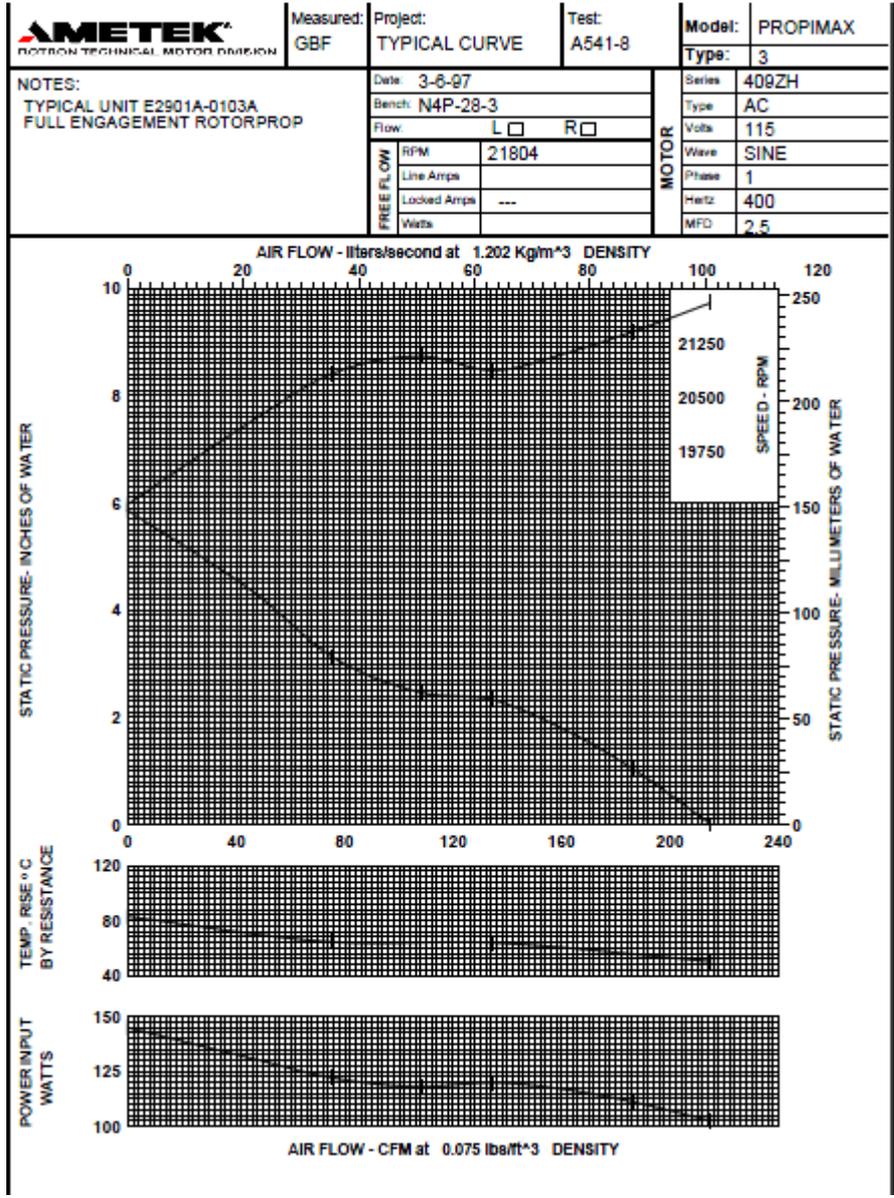

Figure A. 1 POD Experiment AC Fan Geometry [39]

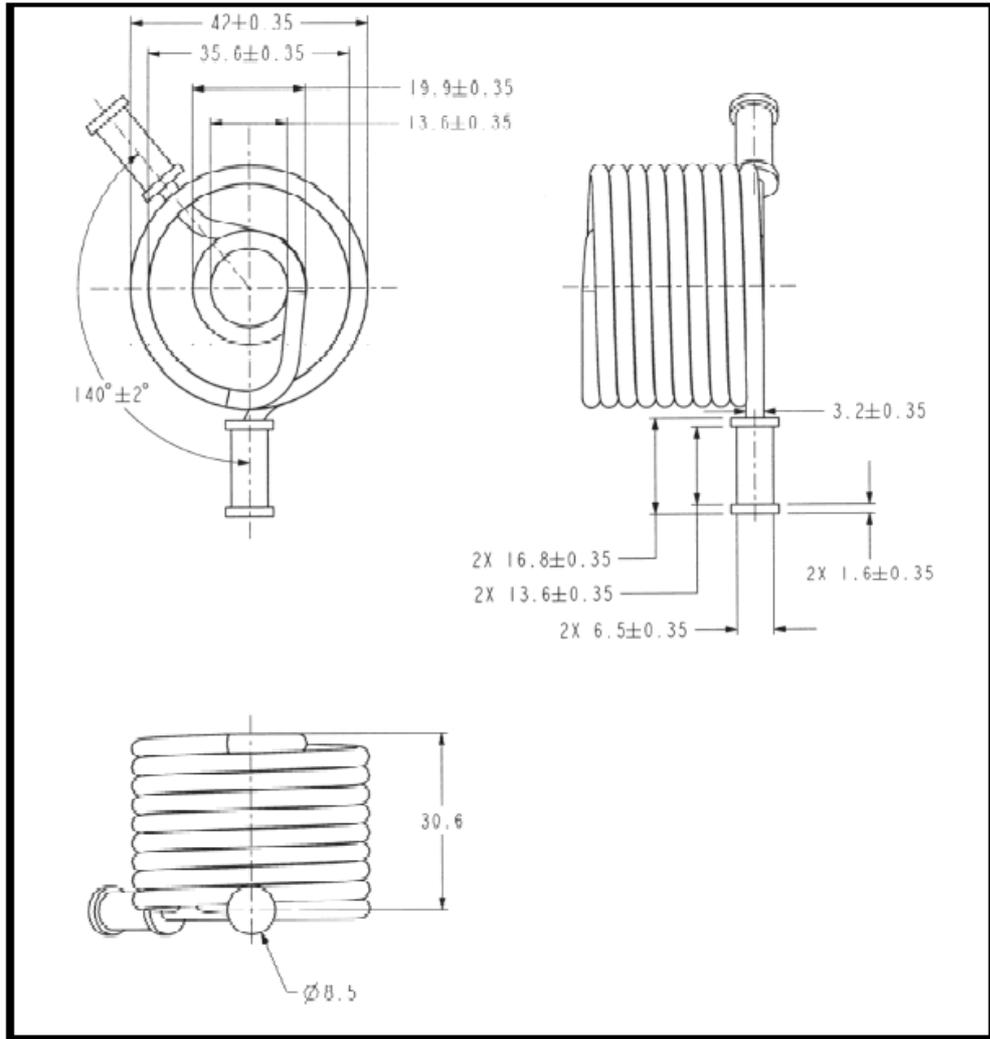Figure A. 2 POD Experiment AC Fan Performance Curve [39]

Figure A. 3 POD Experiment Heater Geometry [40]

Table A. 1 Experiment #4 Input Parameters

Experiment #4	Electrically 2 series 2 parallel TECs (2SX2P TEC)					
Input Data	T_{amb} (°C)	P_e (W)	V_{fan} (V)	V_{flow} (m^3 / min)	R_{set} (Ω)	T_{set} (°C)
	40	50	115 V- 400 Hz	2.97	4.52	44.0

Table A. 2 Experiment #4 Temperature Records versus Time

Time (s)	T10 (°C)	T11 (°C)	T12 (°C)	T13 (°C)	T14 (°C)	T15 (°C)
0	32.38	37.98	39.70	50.04	50.08	49.32
10	32.49	37.85	39.57	50.08	50.09	49.32
20	32.50	37.75	39.45	50.10	50.10	49.34
30	32.54	37.66	39.33	50.12	50.11	49.36
40	32.45	37.56	39.24	50.14	50.13	49.38
50	32.45	37.46	39.15	50.17	50.17	49.40
60	32.50	37.38	39.09	49.87	50.15	49.40
70	32.54	37.31	39.21	47.92	49.88	49.56
80	32.54	37.34	39.44	46.72	49.93	50.19
90	32.61	37.45	39.67	46.30	50.20	50.92
100	32.70	37.59	39.92	46.13	50.42	51.48
110	32.71	37.71	40.18	46.02	50.56	51.89
120	32.65	37.89	40.51	45.88	50.60	52.17
130	32.59	38.10	40.84	45.75	50.56	52.31
140	32.61	38.29	41.19	45.56	50.45	52.34
150	32.57	38.54	41.53	45.37	50.33	52.30
160	32.29	38.78	41.89	45.20	50.19	52.22
170	32.05	39.01	42.20	45.03	50.03	52.12
180	32.20	39.24	42.52	44.87	49.87	51.98
190	32.18	39.50	42.85	44.71	49.73	51.87
200	32.10	39.76	43.13	44.61	49.61	51.74
210	32.04	39.98	43.40	44.48	49.49	51.64
220	31.97	40.24	43.67	44.41	49.44	51.57
230	32.13	40.47	43.91	44.34	49.35	51.48
240	32.31	40.70	44.16	44.29	49.29	51.40

|					
250	32.32	40.89	44.37	44.25	49.23	51.34
260	32.22	41.12	44.58	44.20	49.18	51.28
270	32.16	41.31	44.81	44.16	49.13	51.23
280	32.07	41.48	44.99	44.10	49.08	51.16
290	32.23	41.68	45.18	44.06	49.05	51.13
300	32.41	41.87	45.37	44.03	49.03	51.10
310	32.47	42.05	45.56	44.00	49.00	51.06
320	32.28	42.22	45.74	43.96	48.97	51.03
330	32.16	42.39	45.90	43.94	48.94	50.99
340	32.01	42.57	46.10	43.92	48.94	50.97
350	32.11	42.70	46.27	43.88	48.90	50.94
360	32.24	42.87	46.45	43.87	48.89	50.92
370	32.19	43.00	46.57	43.82	48.86	50.89
380	32.18	43.15	46.76	43.80	48.83	50.84
390	32.39	43.32	46.91	43.78	48.83	50.81
400	32.41	43.46	47.07	43.78	48.82	50.78
410	32.35	43.60	47.22	43.75	48.81	50.76
420	32.47	43.75	47.35	43.71	48.79	50.72
430	32.26	43.88	47.51	43.69	48.76	50.71
440	32.35	44.01	47.65	43.67	48.74	50.68
450	32.33	44.15	47.79	43.64	48.72	50.66
460	32.24	44.27	47.94	43.62	48.71	50.62
470	32.35	44.38	48.06	43.60	48.69	50.59
480	32.31	44.50	48.18	43.58	48.67	50.56
490	32.27	44.64	48.34	43.56	48.65	50.55
500	32.45	44.76	48.48	43.53	48.62	50.51
510	32.41	44.89	48.61	43.50	48.60	50.50
520	32.32	45.01	48.73	43.49	48.58	50.48
530	32.51	45.11	48.85	43.47	48.55	50.45
540	32.65	45.24	48.98	43.43	48.53	50.41
550	32.63	45.38	49.12	43.42	48.52	50.40
560	32.62	45.49	49.27	43.40	48.51	50.38
570	32.64	45.62	49.38	43.39	48.50	50.36
580	32.61	45.73	49.50	43.37	48.49	50.32
590	32.55	45.84	49.61	43.36	48.47	50.31
600	32.48	45.94	49.73	43.34	48.45	50.29
610	32.65	46.06	49.88	43.33	48.45	50.26
620	32.75	46.17	50.00	43.30	48.44	50.23
630	32.59	46.28	50.12	43.30	48.42	50.22
640	32.61	46.40	50.23	43.27	48.40	50.21
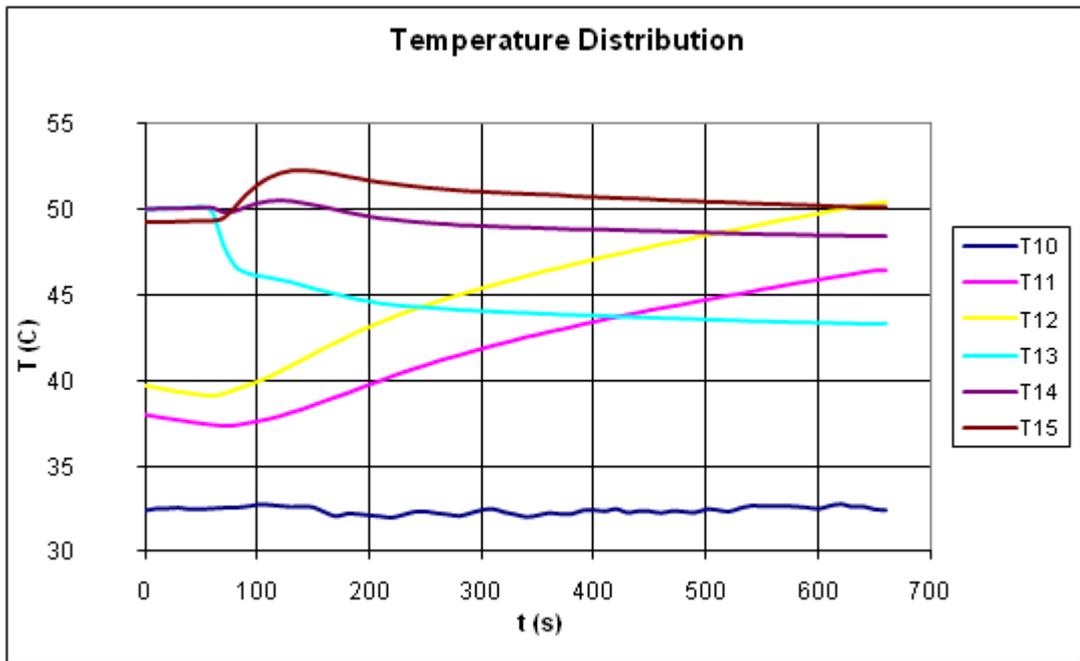
Figure A. 4 Temperature Variations of the Controlled Regions of Experiment #4